To the Graduate Council:

I am submitting herewith a thesis written by Alfredo Gabrie entitled "An experimental Study of Vortex Surface Interactions and 3-D Optical Topographic Mapping." I have examined the final copy of this thesis for form and content and recommend that it be accepted in partial fulfillment of the requirements for the degree of Master of Science, with a major in Mechanical Engineering.

Dr. Ahmad Vakili, Major Professor

We have read this thesis
and recommend its acceptance:

Dr. J. M. Wu

Dr. R. Roach

Accepted for the Council:

Associate Vice Chancellor
and Dean of The Graduate
School

STATEMENT OF PERMISSION TO USE

In presenting this thesis in partial fulfillment of the requirements for a Master's degree at The University of Tennessee, Knoxville, I agree that the Library shall make it available to borrowers under rules of the Library. Brief quotations from this thesis are allowable without special permission, provided that accurate acknowledgment of the source is made.

Permission for extensive quotation from or reproduction of this thesis may be granted by my major professor, or in his absence, by the Head of the Interlibrary Services when, in the opinion of either, the proposed use of the material is for scholarly purposes. Any copying or use of the material in this thesis for financial gain shall not be allowed without my written permission.

Signature Alfredo Gabrie.

Alfredo Gabrie

Date 4/12/94

AN EXPERIMENTAL STUDY

OF

VORTEX SURFACE INTERACTIONS

AND

3-D OPTICAL TOPOGRAPHIC MAPPING

A Thesis

Presented for the

Master of Science

Degree

The University of Tennessee, Knoxville

Alfredo Gabrie

May 94

DEDICATION

This thesis is dedicated to my parents

Olga J. Salles Vega de Gabrie

and

Alfredo Salvador Gabrie Paranky.

"Siempre Vivira"

who have provided me with constant support and with great educational opportunities throughout my life.

ACKNOWLEDGMENTS

This work was performed under support from DARPA with additional support by the UTSI research and proposal development funds. I would like to take this opportunity to express my sincere appreciation to those who have made this investigation possible. The author would like to thank his academic advisor, Dr. A. Vakili, for devising the three-dimensional non-intrusive surface reconstruction technique, and for his continuous support in performing this study. His knowledge and wisdom were invaluable to carry out this project. Dr. Vakili was enthusiastic and energetic about the subject, and he was always willing to overcome any type of difficulties obstructing the development of the project. His performance have far exceeded my expectations.

I would like to thank Dr. J. M. Wu for selecting me in the Fall of 1992 as a team member of the O.S.D.P., for sharing his invaluable experience, and for his guidance as a member of my thesis committee. Also, I would like to thank Dr. R. Roach for his advice and recommendations concerning the graphics and numerical methods implemented in this project. Dr. Roach was always available even during late hours in the evening. I also appreciate the time and technical discussions with Dr. K. Kimble and Dr. J. Z. Wu.

I would like to thank G. Z. Shi, W. Y. Jiang, and X. H. Wu for developing the FORTRAN code for the Inviscid Linearized Theory, and for allowing me to implement their results into my research.

I would like to thank Scott Meredith and Chris Pipe, who are also graduate research assistants working for the O.S.D.P., for their suggestions and comments throughout the investigation.

I would like to thank the staff at the library for their support during the literature search. Finally, I would like to thank the technicians at the UTSI Machine Shop, and at the Fluid Dynamic Laboratories for the construction and maintenance of the experimental set up and facilities. Specially to Mr. Ricky Meeker for his continuous technical support during the experiments.

ABSTRACT

This document describes the results of an experimental study on vortex surface interactions. The experimental study was performed to help establish a complete understanding of the vortex surface fluid physics necessary to comprehend the surface signature generated by a submerged body. Results showed that higher Froude numbers resulted in stronger surface signatures. The behavior and development of the vortex surface interaction were consistent with observations reported previously. The Alternate Linearization Method showed that the surface signature is generated by the vortex surface interaction, with the surface pattern not strongly dependent on the surface tension. Preliminary experiments also showed the wave pattern is not strongly dependent on the surface tension.

During the course of the investigation the need for a non-intrusive three-dimensional surface measurement technique was determined. As a result, this study also focused on the design, development, and applications of a new surface measurement and reconstruction technique. The new method was mathematically developed into a unique surface reconstruction technique also useful for other applications, such as machine vision. Preliminary analyses indicate that this new approach has the capability to rapidly map the topography of moving surfaces. This method may be used to determine the topography and velocity of a moving fluid surface. Such information is then useful for better understanding of vortex surface interactions, and as boundary conditions for numerical codes.

PREFACE

In most of the studies conducted in the past as evidenced from a literature review only general features of the vortex free surface interactions have been studied. From our point of view, it is essential to investigate the precise structure of these interactions. In order to understand these structures, their behavior must be identified through their full documentation. The motion of surface elements as well as the flow field near the surface must be quantitatively measured and described.

The study consists of three different parts. First, a review of a theoretical simulation of a vortex pair approaching a free surface depicts the physics and different parameters implicated during the interaction. Second, the design and qualitative study of an experimental simulation in a free surface water tunnel explains the origin and evolution of surface signatures. Third, due to the deficiencies associated with the measurement instrumentation necessary to obtain the specific data, the design development and simulation are described for a new optical topographic mapping technique. This technique is used to determine the surface shape and velocity field near the surface of an incompressible flow. The design and development of the 3-D non-intrusive measurement technique represents a significant breakthrough in this type of investigations. These efforts are complementary to each other, and they provide the basic tools necessary to develop a better understanding of the origin and evolution of surface signatures generated by submerged bodies. The measurements and findings will also provide the foundation for the overall description of particular flow features which

will in turn establish the interface with image and signal processing and detection efforts.

This thesis is divided in two parts. Part I. describes the Vortex Surface Interactions, and Part II. introduces the 3-D Optical Topographic Mapping System.

TABLE OF CONTENTS

PART I: VORTEX SURFACE INTERACTIONS

I. INTRODUCTION **2**

1. BACKGROUND 2

2. LITERATURE REVIEW 3

II. MATHEMATICAL MODELING **7**

1. OBJECTIVE 7

2. PHYSICAL MECHANISM 7

3. GOVERNING EQUATIONS 8

4. BOUNDARY CONDITIONS 9

5. ALTERNATE LINEARIZATION METHOD 10

6. SUMMARY OF NUMERICAL MODEL 11

7. SURFACE TENSION EFFECTS 12

8. VALIDITY AND LIMITATION 13

9. RESULTS 14

III. DESCRIPTION OF EXPERIMENT **15**

1. DESIGN OF EXPERIMENTAL STUDY 15

1.1. OBJECTIVE *15*

1.2. RELATIONSHIP TO REAL BODIES *15*

1.3. FACILITY *16*

1.4. DESIGN CRITERIA *17*

1.5. VORTEX GENERATOR *17*

1.5.1. Tunnel Brackets 18

1.5.2. Main Plates 18

1.5.3. Alpha Plate and Alpha Shaft 18

1.5.4. Wing Section Main Body 19

1.5.5. Wing Section End-Cover 19

1.5.6. Splitter Plates 20

1.5.7. Fitting Plate 20

1.5.8. Ensemble Procedure 20

2. COMPUTER MODEL 21

2.1. OBJECTIVE *21*

2.2. DIMENSIONLESS PARAMETERS *21*

2.3. INDUCED VELOCITY *22*

2.4. INITIAL VORTEX STRENGTH *23*

2.5. SUMMARY *24*

2.6. ANALYSIS *25*

3. QUALITATIVE TEST PROCEDURE 26

3.1. FLEXIBILITY *26*

3.2. PRELIMINARY SETTINGS *26*

3.3. TEST PROCEDURE *27*

4. SURFACE TENSION EFFECTS 28

IV. MEASUREMENTS **29**

1. OBJECTIVE 29

2. QUALITATIVE MEASUREMENTS AND OBSERVATIONS 29

2.1. VORTEX PAIR DEVELOPMENT, VORTEX VORTEX INTERACTION *30*

2.2. DEVELOPMENT OF SURFACE SIGNATURE, SURFACE VORTEX INTERACTION *30*

3. INSTRUMENTATION 31

PART II: 3-D OPTICAL TOPOGRAPHIC MAPPING

V. INTRODUCTION 33

1. BACKGROUND 33

1.1. FLUID DYNAMICS 33

1.2. MACHINE VISION SYSTEM 33

2. STATE-OF-THE-ART LITERATURE REVIEW 34

VI. SYSTEM DESCRIPTION 37

1. OBJECTIVE 37

2. BASIC DETAIL OF THE CONCEPT 37

3. BASIC HARDWARE DESCRIPTION 39

3.1. ACTIVE CAMERA 39

3.2. PASSIVE CAMERA 39

3.3. RELATIVE DISPLACEMENT MECHANISM 40

VII. CONCEPT DEVELOPMENT 41

1. MATHEMATICAL MODEL 41

2. ANALYSIS 43

3. COMPUTER SIMULATION 44

3.1. OBJECTIVE 44

3.2. ACTIVE CAMERA 45

3.3. PASSIVE CAMERA 45

3.4. METHODOLOGY 45

3.4.1. Projection of Laser Array Pattern 46

3.4.2. Reflection of Laser Array Pattern 47

4. RECONSTRUCTION 48

5. NUMERICAL TECHNIQUES 49

VIII. RESULTS 50

1. ANALYSIS 50

2. RESULTS 52

IX. CONCLUSION 53

LIST OF REFERENCES 55

APPENDICES 59

1. LIST OF FIGURES 60

2. LIST OF TABLES 93

VITA 96

LIST OF FIGURES

FIG. 1. SIGNATURE GENERATED BY A SUBMERGED BODY. 61

FIG. 2. SYNTHETIC APERTURE RADAR (SAR) IMAGES. 62

FIG. 3. PICTORIAL REPRESENTATION OF THE PHYSICAL PROCESSES INVOLVED IN THE GENERATION, INTERACTION AND DISSIPATION OF INTERNAL WAVES. [32] 63

FIG. 4. VORTICES GENERATED BY A SUBMERGED MOVING BODY. [1] 64

FIG. 5. SIMPLIFIED MODEL. BASIC PARAMETERS INVOLVED DURING THE EXPERIMENTAL AND MATHEMATICAL SIMULATION 64

FIG. 6. COUNTER ROTATING VORTEX INTERACTION AND SURFACE DEFORMATION. MATHEMATICAL MODELING. (FR=0.125, S/Λ=2.5, D/Λ=1.25) [14] 65

FIG. 7. SURFACE TENSION EFFECTS ON THE VORTEX SURFACE INTERACTION. MATHEMATICAL MODELING. (FR=0.3, S/Λ=1, D/Λ=3, T=0.3) [14] 65

FIG. 8. THREE-DIMENSIONAL SURFACE SIGNATURE GENERATED BY THE VORTEX SURFACE INTERACTION. (FR=0.1, S/Λ=1, D/Λ=3) [14] 66

FIG. 9. EXPERIMENTAL SET UP. OBJECTIVE IS TO GENERATE STRONG VORTICES IN ORDER TO PRODUCE A 3-D SURFACE SIGNATURE 67

FIG. 10. EXPERIMENTAL SET UP. ENGINEERING DRAWINGS. MAINPLATE. 68

FIG. 11. EXPERIMENTAL SET UP. ENGINEERING DRAWINGS. WING SECTION. 69

FIG. 12. EXPERIMENTAL SET UP. ENGINEERING DRAWINGS. MISCELLANEOUS. 70

FIG. 13. TUNNEL BRACKETS. 71

FIG. 14. MAIN PLATE. 71

FIG. 15. ALPHA PLATE AND ALPHA SHAFT. 72

FIG. 16. WING SECTION MAIN BODY. 72

FIG. 17. WING SECTION END COVER 73

FIG. 18. SPLITTER PLATES. 73

FIG. 19. WING SECTION END COVER, WING SECTION MAIN BODY, AND DYE INJECTOR TUBES. 74

FIG. 20. WING SECTION END COVER, WING SECTION MAIN BODY, SPLITER PLATE, AND DYE INJECTOR TUBES 74

FIG. 21. ALPHA PLATE, ALPHA SHAFT, WING SECTION MAIN BODY, WING SECTION END COVER, SPLITTER PLATE, AND DYE INJECTOR TUBE. 75

FIG. 22. MAIN PLATE, ALPHA PLATE, ALPHA SHAFT, WING SECTION MAIN BODY, WING SECTION END COVER, SPLITTER PLATE, AND DYE INJECTOR TUBE. 75

FIG. 23. EXPERIMENTAL SET UP INSTALLED AT THE TEST SECTION. DIFFERENT PERSPECTIVES. 76

FIG. 24. COUNTER ROTATING VORTICES GENERATED BY THE EXPERIMENTAL MODEL. 78

FIG. 25. VORTEX CORE SEPARATION VS. FROUDE NUMBER 80

FIG. 26. VORTEX CORE SEPARATION VS. INDUCED VELOCITY. 80

FIG. 27. LOCATION AT WHICH QUALITATIVE DATA IS RECORDED. 81

FIG. 28. LASER SHEET CONFIGURATION.
THE LASER HIGHLIGHTS THE COUNTER ROTATING VORTEX PAIR. 82

FIG. 29. SURFACE TENSION EFFECTS. PRELIMINARY SETTINGS. 83

FIG. 30. EVOLUTION AND DEVELOPMENT OF VORTEX PAIR. (D_o/ B_o=1.72, AO=10, V=5 IN./S.). 84

FIG. 31. DEVELOPMENT OF SURFACE SIGNATURE. (D_o/ B_o=1.72, A_o=10, V=5 IN./S.). 86

FIG. 32. 3-D SURFACE SIGNATURE. (D_o/ B_o =1.72, A_o=10, V=5 IN./S.). 87

FIG. 33. SCHEMATIC, OPTICAL TOPOGRAPHIC MAPPING. 88

FIG. 34. EXPERIMENTAL, OPTICAL TOPOGRAPHIC MAPPING. 89

FIG. 35. ACTIVE CAMERA. PROJECTS A LASER BEAM ARRAY. 90

FIG. 36. PASSIVE CAMERA. CCD CAMERA. CAPTURES THE REFLECTION. 90

FIG. 37. MATHEMATICAL COORDINATES, OPTICAL TOPOGRAPHIC MAPPING. SINGLE RAY. 91

FIG. 38. BASIC RECONSTRUCTION ALGORITHM 91

FIG. 39. SIMULATION, "3DOTS", THREE DIMENSIONAL OPTICAL TOPOGRAPHIC SYSTEM. 92

LIST OF SYMBOLS

3DOTS.....3-D Optical Topographic System

ALM.....Alternate Linearization Method

AR.....Aspect Ratio

b_0.....Initial Vortex Core Separation

c_i.....Complex Location of the Vortex Below the Rigid Surface

D_0.....Initial Vortex Depth of Vortex Pair

Fr.....Froude number

g.....Gravitational Constant

$PF_{x,y,z}$.....Coord. of Projection Focal Point, 3-D Space

$PM_{x,y}$.....Coord. of ith Beam in the 2-D Proj. Plane

r.....Position Vector

$RF_{x,y,z}$.....Coord. of Reflection Focal Point, 3-D Space

$RM_{x,y}$.....Coord. of ith Beam in the 2-D Reflec. Plane

$RS_{x,y,z}$.....Coord. of ith Beam, 3-D Space

t.....Time

V.....Velocity Distribution Vector

V_o.....Net Induced Velocity

x, y.....Coordinate Axes, x at Free Surface in Lateral Direction, y Downward Plus

z_i.....Location of the Vortex, $x_i + iy_i$

α_0.....Initial Angle of Attack

Γ.....Vortex Circulation

η.....Free Surface Elevation Above Still Surface Level

λ.....Background Wave Length

Ω.....Vorticity

Φ.....Velocity Potential

ε.....Perturbation Parameter

PART I: VORTEX SURFACE INTERACTIONS

CHAPTER I.

INTRODUCTION

1. BACKGROUND

A submerged moving body usually generates (fluid mechanic) signatures which contain vortices, pressure waves, and turbulence,[1] Fig. 1*. Vortices are orderly and coherent rotational structures in fluid motion. Vortices created from the hull, control surfaces, propellers, etc., are not only interacting with each other but are sometimes also interacting with the water surface. Thus, they leave a particular surface structure "signature" on the surface which may be detected by modern remote sensing techniques coupled with proper image and pattern recognition processes. Synthetic Aperture Radar (SAR) images show a ship's wake as a narrow dark band bordered by two bright lines Fig. 2. The dark band is detectable many kilometers downstream at all angles to the SAR azimuth direction even under severe weather conditions. On the other hand two bright lines appear only in light winds.[2] A complete investigation of the physical process leading to understanding the structure of the SAR images is necessary in order to refine the detection techniques of submerged bodies. Consequently, a detailed study of the interaction of vortices with each other and with the surface is necessary to define the signature searched by SAR.

---

* All figures may be found in the appendix.

The status of a sea surface can vary from a quite mirror-like surface to a very stormy and rough one, full of small to giant waves, caused by the wind, tidal, rain, sea current influenced by the geographical structure of the sea shore, and sea-bed shapes, etc., Fig. 3. The inertial gravity, temperature, density, surface tension, viscous effects, etc., do influence the surface signature. The propagation of generated disturbances are also a function of buoyancy, density, level of stratification of water, etc. The problem may be even more complex when all of the above are occurring in a shallow sea. It is known that the depth of a sea-bed will significantly amplify the waves. This offers a better chance for detection, but it is also contributing to a tremendously intensified background noise level which make it more difficult to observe signatures.

To develop a quantitatively complete and accurate understanding of the fluid mechanics problems involved, an experimental study of the mechanism responsible for the signature created by a submerged body is necessary under controlled environmental surroundings.

2. LITERATURE REVIEW

In order to develop a good understanding of the interactions between the multiple vortices generated by a submerged moving body and the free surface, Fig. 4, simplified models have been constructed over the years by the researchers in this field. In this case the interaction of a counter-rotating vortex couple will be simulated as a model for the numerous vortices generated by a real body. The counter rotating vortex pair is the most common and simplest wake model, which can be employed as

foundation for the understanding of more complex turbulent wake flow interaction with the free surface.

Controlled laboratory experiments regarding the signature generated by free surface vortex couple interaction have been conducted since 1983. For example, a rectangular delta wing moving parallel to the surface generates a vortex couple which subsequently interacts with the free surface. The principal surface disturbances observed are termed Scars and Striations. [3, 4, 5] Striations are three dimensional surface disturbances which appear abruptly perpendicular to the path of the model. Striations usually grow to about three times the initial vortex core separation (b_0), and they start to appear when the vortex pair is one spacing b_0 from the surface. Scars are small depressions on the free surface comprised of many randomly distributed whirls which start at the end of the Striation phase. The origin, development, and behavior of Scars and Striations are additional areas of research regarding free surface vortex couple interaction.

Striations are generated by the short wave length instability of the vortex pair, and the helical instability of tightly spiraled regions of vorticity. [6, 7, 8] The instabilities come into existence even without a free surface. The Striations are a consequence of the interactions of the instabilities with the free surface. The experimental results also suggest the whirls originate from the interaction of Striations with surface vorticity, and the whirls-merging process is responsible for the creation and persistence of Scars.

Early in 1992 Sarpkaya [9] reported the observations of an experiment in which he studied the interaction of a single turbulent trailing vortex and its image with a free surface. The vortex was generated in a water tunnel through the use of a hydrofoil. The purpose of

the experiment was to further explore the origin of Scars, Striations, and the three dimensional instabilities. The results indicate that a series of vortex sheets stretched out of the vortex core due to the helical instabilities. The exchange of momentum between the outer regions and the core generates the short wave length instabilities. The vortex sheets thrown away from the vortex core interact with the free surface forming whirls, or move tangentially to dissipate quickly.

Three-Dimensional surface deformations generated by a vortex couple have been confirmed by different studies. The results also show that the vortices are deflected as they approach the free surface. The vortex pair is deflected in a way similar to vortices approaching a solid surface. Hence, there is vorticity generation at the free surface.[10,11] Vorticity is generated during the vortex interaction with the free surface; however, the effects of surface conditions have not been taken into account. Flow visualization studies regarding surface tension and surface conditions indicate that surface, or capillary effects are important. The vortex interaction with a contaminated free surface results in the generation of secondary and tertiary vortex rings that limit the outward motion of the vortex ring core.[12] The vortex interaction with a cleaner surface results in a much larger outward motion of the vortex ring core, and the generation of secondary vorticity is delayed. The results indicate that the surface tension, or capillary effects are important. The surface tension is directly proportional to the vorticity generation, and inversely proportional to the outward motion at the free surface.

The previous studies have been conducted on free surfaces which do not contain any type of motion. For most practical purposes the water contains some type

of motion or background disturbances, which may significantly affect the current observations. Fish[13] in 1990 reported the results of experiments on vortex pairs moving toward a free surface containing waves. Two vertical rotating flaps were used to generate a vortex pair, and then two dimensional waves were generated with an oscillating plate type wavemaker. There is evidence of a strong interaction between the waves and the vortex trajectory. Flow visualization results show elimination of the rebounding effect on the upstream traveling vortex, and an increase in the rebounding effect on the downstream vortex. Technically, each vortex is attracted to the shear layer that will improve their existence. The right side vortex (c.w. vorticity) moves closer to the free surface to take advantage of the thin shear layer (c.w. vorticity) created by the movement of the waves; however, the left vortex (c.c.w. vorticity) rebounds to remain in the opposite sign shear layer below the thin surface region.

There are several numerical techniques available in the literature which are capable of simulating the vortex couple free surface interaction. A wide range of theoretical and numerical study has been performed in this area during the last few years.[14] Different efforts are reviewed by Sarpkaya.[2] Lugt's group[15,16] studied the viscous free surface interaction, Tryggvason[17] elaborated in the inviscid nonlinear free surface interactions, and Fish[18] as well as King[19] investigated the inviscid linearized free surface interaction. A numerical simulation initially developed by Fish[18] and then improved by G. Z. Shi, W. Y. Jiang, and X. H. Wu[14] will be reviewed in the following chapter.

CHAPTER II.

MATHEMATICAL MODELING

This is a review of the work performed by G. Z. Shi, W. Y. Jiang, and X. H. Wu[14] in support of the current investigation.

1. OBJECTIVE

The purpose of the mathematical simulation is to generate the surface signature produced by a submerged moving body, to show that vortex surface interactions effectively leave a pattern at the free surface, and to investigate the dominant parameters in the flow.

The linearized inviscid theory developed by Fish[18] is capable of simulating a simplified model of the surface signature generated by a submerged moving body.[14] The linearized inviscid theory developed by Fish applies an Alternate Linearization Method (ALM) to the traditional surface boundary conditions. G. Z. Shi, W. Y. Jiang, and X. H. Wu[14] developed a FORTRAN code implementing and improving the inviscid linearized theory. They developed a numerical filter which allows the code to run for a longer period of time. The numerical results presented in this section were obtained by G. Z. Shi, W. Y. Jiang, and X. H. Wu.

2. PHYSICAL MECHANISM

The flow of a free surface with waves can usually be considered inviscid since the Reynolds number is large, and compressibility effects are neglected since the

induced velocities in the free surface vortex flows are small.[20] A 2-D simulation will be implemented because a full 3-D simulation is too complex, this will result in a significant reduction in the complexity of the problem. The two-dimensional simulation is based on the assumption that the velocity gradients along the axis of the ship are small, and that a two dimensional flow description in a plane normal to the ship axis may be integrated in time and stacked in space using constant ship speed to represent the three-dimensional problem.[18]

Figure 5 shows a pair of counter rotating vortices and the different parameters involved during the simulation. The ambient waves propagate from left to right transverse to the submerged body motion.

3. GOVERNING EQUATIONS

The flow is inviscid and incompressible. The fluid motion can also be considered irrotational, since the vortex pair has concentrated vorticity. It is a circulatory flow without rotation. The continuity equation for an incompressible flow is,

$$\nabla \cdot \mathbf{V} = \mathbf{0} \tag{1}$$

and the condition of irrotationality is,

$$\boldsymbol{\Omega} \equiv \nabla \times \mathbf{V} = \mathbf{0} \tag{2}$$

Eq. (2) ensures the existence of a scalar function of position and time,

$$\Phi = \Phi(\mathbf{r}, t) \tag{3}$$

such that,

$$\mathbf{V} = \nabla\Phi \tag{4}$$

where Φ is the velocity potential. Hence, combining Eqs. (1) and (4) the following relationship is obtained,

$$\nabla \cdot \nabla\Phi = \nabla \cdot \mathbf{V} = \nabla^2\Phi = 0 \tag{5}$$

which is the Laplace's equation. Hence, the governing expression for the counter rotating vortex pair rising to the free surface is the Laplace's equation.

4. BOUNDARY CONDITIONS

There are two types of boundary conditions: Kinematic and Dynamic. The only assumptions used are that the fluid is ideal (inviscid and incompressible), the surface tension is negligible, and the velocity gradients along the axis of the submerged moving body are small (2-D).

A Cartesian coordinate system will be used, Fig. 5. The plane of the undisturbed water surface is at the x-z plane with y = 0. Hence, the vertical surface elevation, y, can be defined as $y = \eta(x, z, t)$. Since the fluid motion is 2-D $y = \eta(x, t)$.

The Kinematic boundary condition is based on the fact that the total derivative of the quantity $y - \eta$ vanishes at the free surface.[20] In other words, the normal velocities of the fluid and of the boundary surface must be equal. Hence, at $y = \eta$,

$$\frac{D}{Dt}(y - \eta) = \frac{\partial \Phi}{\partial y} - \frac{\partial \eta}{\partial t} - \frac{\partial \Phi}{\partial x}\frac{\partial \eta}{\partial x} = 0 \tag{6}$$

The dynamic boundary condition is based on Bernoulli's equation for unsteady irrotational flows.[20] The physics behind the dynamic boundary conditions is that the pressure on the free surface must be atmospheric. At $y=\eta$,

$$\frac{\partial \Phi}{\partial t} + \frac{1}{2}\nabla \Phi \cdot \nabla \Phi + \frac{\eta}{F^2} = 0 \tag{7}$$

where the following non-dimensionalization for Eqs. (6) and (7) has been used,

$$Fr = \frac{\Gamma}{\left(g\lambda^3\right)^{1/2}}, \quad \Phi = \frac{\Phi'}{\Gamma}, \quad \eta = \frac{\eta'}{\lambda}, \quad t = \frac{t'\Gamma}{\lambda^2} \tag{8}$$

The boundary conditions are linearized using the Alternate Linearization Method (ALM) while maintaining the adequate physics of the flow.

5. ALTERNATE LINEARIZATION METHOD

The Alternate Linearization Method (ALM), developed by Fish[18], is based on the inviscid linearized theory. The ALM employs a 0th order solution which is more accurate than the classical free surface flow liearizations for flows with submerged point vortices of low Froude numbers. After linearizing the boundary conditions are expresses as,

Dynamic,

$$\frac{\partial \Phi}{\partial t} + \frac{1}{2}\left(\frac{\partial \Phi}{\partial x}\right)^2 + \frac{\eta}{\varepsilon} = 0 \tag{9}$$

Kinematic,

$$-\frac{\partial \Phi}{\partial y} + \frac{\partial \eta}{\partial t} + \frac{\partial \Phi_0}{\partial x}\frac{\partial \eta}{\partial x} - \eta\frac{\partial^2 \Phi_0}{\partial y^2} = 0 \tag{10}$$

These two linearized boundary conditions and Laplace's equation are employed to numerically model the vortex pair free surface interaction problem. This technique is only valid for small Froude numbers (Fr < 0.5).

6. SUMMARY OF NUMERICAL MODEL

The governing equations and boundary conditions for the modeling of the surface signature generated by a submerged body are expressed as,

Governing Equation:

$$\nabla^2\Phi = 0 \tag{11}$$

Boundary Conditions at y = 0:

$$\frac{\partial \Phi}{\partial t} + \frac{1}{2}\left(\frac{\partial \Phi}{\partial x}\right)^2 + \frac{\eta}{\varepsilon} = 0 \tag{12}$$

$$-\frac{\partial \Phi}{\partial y} + \frac{\partial \eta}{\partial t} + \frac{\partial \Phi_0}{\partial x}\frac{\partial \eta}{\partial x} - \eta\frac{\partial^2 \Phi_0}{\partial y^2} = 0 \tag{13}$$

Assumptions:

- Inviscid
- Incompressible
- Irrotational
- 2-D
- Small Froude number
- Negligible Surface Tension
- Uniform Atmospheric Pressure at the free surface
- Vortex couple reaches free surface

7. SURFACE TENSION EFFECTS

Several researchers believe that surface tension effects play an important role during the development of the surface signature.[21, 22] In a reality, the surface tension is significantly increased when the vortices arrive to the free surface. The surface tension increases due to the different type of water composition arriving at the surface with the vortex couple.

The ALM code was modified to study the effects of surface tension on the development of the surface signature generated by a submerged body. The major modifications occurred on the dynamic boundary condition, Eq. (7). Initially, the surface tension effects were neglected. G. Z. Shi, W. Y. Jiang, and X. H. Wu[14] implemented the modification of the of dynamic boundary conditions in a computer simulation. Their dynamic boundary condition can be expressed as,

$$\frac{\partial \Phi}{\partial t} + \frac{1}{2}\nabla\Phi \cdot \nabla\Phi + \frac{\eta}{F^2} = \kappa\tau \tag{14}$$

where,

$$\kappa = \kappa\lambda \qquad \tau = \frac{\tau\lambda}{\rho T^2} \tag{15}$$

After linearizing,

$$\frac{\partial\Phi}{\partial t} + \frac{1}{2}\left(\frac{\partial\Phi}{\partial x}\right)^2 + \frac{\eta}{\varepsilon} = \kappa\tau \tag{16}$$

8. VALIDITY AND LIMITATION

The ALM technique provides good results if the Froude number based on the vortex circulation is small; the vortices can reach the surface field before they suffer severe distortion, diffusion and dissipation; and the vortex pair is not too close to the free surface.[14] The numerical errors due to the underlying assumptions are very small, hence the results can be considered accurate.

The Froude number based on the vortex circulation has to be small since the linearization theory eliminates all terms of order ε^2 or greater (ε^2=Fr^4) in the general form of the linearized solution, Eqs. (9) and (10).

The vortex pair is subject to a series of instabilities which might develop before they reach the surface. The instabilities make the vortex couple oscillate until they break into curved segments. The instabilities invalidate the assumption that a two dimensional flow description in a plane normal to the ship axis may be integrated in time and stacked in space using constant ship speed to represent the three-dimensional problem.

If a vortex pair is generated not too far from the free surface a vortex sheet instead of a vortex pair might be interacting with the free surface. A finite span vortex sheet is initially generated by a moving body, then the vortex sheet rolls up and forms a vortex couple.

9. RESULTS

There is a significant signature generated by the interaction of the counter rotating vortices and the free surface. The magnitude of the surface signature is directly proportional to the magnitude of the Froude number. We can say the magnitude of the surface signature is mainly a function of the Froude number and the distance of the vortex couple from the free surface. Figure 6 shows the evolution and interaction of the counter rotating vortices with the free surface.

The surface tension effects are minimum during the wave suppression process. Figure 7 shows that the amplitude of the surface elevation is slightly reduced by the surface tension. Hence, the vortex surface interaction plays a dominant role during the generation of the surface signature. The surface tension might play a significant role during the dissipation time of the surface signature which can not be evaluated with the current numerical technique. Figure 8 shows the three dimensional signature developed by a submerged body.

CHAPTER III.

DESCRIPTION OF EXPERIMENT

1. DESIGN OF EXPERIMENTAL STUDY

1.1. OBJECTIVE

The purpose of the experiment is to generate significant three-dimensional surface signatures. A minimum Froude number of 0.15 based on vortex separation is necessary to generate a significant three-dimensional surface signature according to previous experimental observations made by researchers in this field.[6] A simplified computer model has been developed in order to identify the parameters which meet the criteria of the experiment's objective. This model takes into account the physical constraints of the facility, as well as the long wave instabilities.

1.2. RELATIONSHIP TO REAL BODIES

The surface signature generated during the experiments is the signature which a submerged moving body or a moving ship might generate at the free surface. Figure 2 shows a surface signature generated by a moving ship. The question is to whether or not a submerged body will generate a significant surface signature. It has been experimentally found that a detectable surface signature is generated only for Froude numbers of 0.15 or higher based on the vortex separation. Due to the wide variety of

vortices generated by real body, Fig. 4, it is a difficult task to directly correlate the experimental observations to that of a real body.

For a real body, assuming that the two tip vortices generated by the main hydrofoils are isolated, the Froude number based on the two tip vortices is in the range of 0 to about 0.1. This Froude number is rather small since the vortex separation is relatively large. However, there are other vortices generated by the body which might result in higher Froude numbers. In order to identify which specific vortices travel to the surface and produce the specific signature, a detailed study of the magnitude of the Froude number generated by a real submerged body is necessary. The study can be accomplished by a three-dimensional simulation of a submerged body.

1.3. FACILITY

The experiment is designed to be conducted at The University of Tennessee Space Institute in a low turbulence water tunnel with an open test section with dimensions 18"X12"X60". A 1 inch by 1 inch squared grid is installed on the wall and floor of the water tunnel in order to obtain quantitative analysis of the vortex vortex, and vortex free surface interactions.

The facility has an on-line filtering system which eliminates any type of impurities present in the water prior to any particular test. There are three different pressurized dye reservoirs available for flow visualization, as well as a series of camera rails which facilitate the recording of qualitative data.

1.4. DESIGN CRITERIA

The experimental model needs to generate a counter rotating vortex couple with sufficient vortex strength to generate significant three-dimensional surface deformations; furthermore, the experimental set-up should be flexible and non-intrusive. In addition, the ensemble procedure should be simple and the use of specialized tools should be minimized.

1.5. VORTEX GENERATOR

The model consist of two NACA 0012 vertically mounted rectangular foils with an AR of 1.175. The separation distance between the tip vortices (b_o) and free surface (D_o) may be controlled through a series of simple adjustments, Fig. 9. The experimental set-up is symmetric, and is designed to minimize the water disturbances associated with the different components. The experimental set-up consists of seventeen different parts:

- 4 Tunnel Brackets
- 2 Main Plates
- 2 Alpha Shafts
- 2 Alpha Plates
- 2 Wing Section Main-Body
- 2 Wing Section End-Cover
- 2 Splitter Plates
- 1 Fitting Plate

The engineering design specifications of the experimental set up are included in Figs. 10, 11, and 12.

1.5.1. Tunnel Brackets

They are used to attach the main plates to the wall of the tunnel, and they are designed to fit the contour of the upper section of the tunnel walls. Two brackets are used in each main plate. The upper section of the tunnel wall have a series of threaded holes which allows an individual to move the brackets, and so the experimental model along the open test section of the tunnel. Figure 13.

1.5.2. Main Plates

The main plate is used as an elevator for the airfoils, or vortex generators. The plate has a slot which allows the airfoils to move vertically, and two series of holes which are used to set the angle of attack in conjunction with the alpha plate and shaft. The main plate is aerodynamically designed in order to minimize unwanted water disturbances. The main plate has a height of 11.5 inches and a width of 7 inches. Figure 14.

1.5.3. Alpha Plate and Alpha Shaft

The alpha plate has a series of holes with a 5 degree increment having as a center of curvature the alpha shaft. By aligning the holes in the Alpha Plate with the holes in the main plate the vertical position and angle of attack of the model can be adjusted. The Alpha Shaft is located at the center of curvature corresponding to the series of holes located in the Alpha

Plate. The Alpha Shaft also has a series of holes which are used to vary the spacing between the airfoils. Figure 15.

1.5.4. Wing Section Main Body

The wing section, which consist of two NACA 0012 rectangular foils, are used to generate a pair of vortices. The NACA 0012 airfoils have a span of 5.5 in., and a chord length of 5 in. The vortices can be co-rotating, or counter-rotating depending on the angle of attack and wing position (left, or right). A positive angle of attack on the right side, looking from downstream, generates a c.w. rotating vortex, while a positive angle of attack on the left generates a c.c.w. rotating vortex and vice-versa, Table I*.

The separation between the airfoils is adjusted by pining the wing and the Alpha Shaft together. The airfoils and the pin-holes in the wing are observed in Fig. 16.

1.5.5. Wing Section End-Cover

The Wing Section End-Cover is round in order to reduce the possibility of flow separation, and/or vortex unsteadiness. The End-Cover facilitates the connection of the dye injector tubes, which go through the Wing Section Main Body and then to a pressurized dye reservoir. Figure 17.

---

* All tables may e found in the appendix.

1.5.6. Splitter Plates

The purpose of the Splitter plate is to eliminate the vortex on one side of the wing section. It is also aerodynamically designed in order to minimized unwanted water disturbances. Figure 18.

1.5.7. Fitting Plate

The Fitting Plate is installed at the bottom wall of the tunnel. The Fitting Plate is used to ensure there is not clearance between the Main Plate and the tunnel side walls.

1.5.8. Ensemble Procedure

The Dye Injector tube is connected to the Wing Section End Cover, and then put through the Wing Section Main Body as shown in Fig. 19. The Splitter plate is then installed at the opposite end of the Wing Section End Cover, Fig. 20. The Alpha Shaft and Alpha Plate can now be connected to the wing section as depicted in Fig. 21. Then, the vertical position and angle of attack of the wing section are set by installing the Alpha Plate in the Main Plate, Fig. 22. The main plate is attached to the water tunnel side walls using the tunnel brackets. Then, the fitting plate is installed at the bottom of the tunnel to ensure a zero clearance between the tunnel side walls and the Main Plate.

Figures 23 and 24 show the experimental set up installed at the test section, and different perspectives of the counter rotating vortices respectively. Figure 24 shows that there is evidence of a 3-D surface signature.

2. COMPUTER MODEL

2.1. OBJECTIVE

The purpose of the computer model is to verify the effectiveness of the vortex pair, and to justify the construction of the experimental set up. The simulation attempts to calculate a rough estimate of the magnitude of the Froude number, and to perform a parametric study of the general effects and trends of the different parameters involve during the testing procedure. Specially, α_0, b_0, and D_0 which showed to have a significant effect on the surface signature during the mathematical modeling.

2.2. DIMENSIONLESS PARAMETERS

The crucial dimensionless parameter in the current experiment is the Froude number which represents the ratio of inertial force to gravity force. The Froude number is directly proportional to the magnitude of the surface deformation. The inertial force is a function of the vortex strength or circulation. During the experiments, the Froude number is defined as,

$$Fr = V_0 / \sqrt{g b_0} \tag{17}$$

Then, the Froude number is a function of the mutual induced velocity (V_0) generated by the counter rotating vortices, and the vortex core separation (b_0).

2.3. INDUCED VELOCITY

The induced velocity is the magnitude of the velocity generated by each vortex on the other vortex. The vortex pair rises to the surface due to the fact that the induced velocity vector has a direction pointing toward the free surface. The induced velocity can be estimated from the definition of circulation or Biot-Savart Law. The circulation or vortex strength Γ of a velocity field $\mathbf{V}$ is defined as the line integral of the velocity field around any closed curve C, hence,

$$\Gamma_C = \oint_C \mathbf{V} \cdot \mathbf{ds} \tag{18}$$

If a point vortex or concentrated vorticity is assumed to be in the flow, the velocity field vector will only have one component u_θ, which is only a function of r. By converting Eq. (18) to polar coordinates,

$$\Gamma_C = \oint_C u_\theta \, r \, d\theta \tag{19}$$

thus,

$$\Gamma_C = u_\theta \, 2\pi r, \text{ or} \tag{20}$$

$$V_o = \frac{\Gamma}{2\pi b_o} \tag{21}$$

where u_θ is the magnitude of the net induced velocity. This approximation is only valid for incompressible an irrotational flows. If the fluid motion can be considered inviscid and the flow is subject to irrotational forces the material rate of change of circulation

around any surface element moving with the fluid is permanently zero, Kelvin Vorticity Theorem.

2.4. INITIAL VORTEX STRENGTH

A NACA 0012 can be considered a thin symmetric wing section. Then, the vortex strength can be calculated by the classical Thin Airfoil Theory. For thin airfoils the camber line can be simulated by a vortex sheet placed along the camber line. This is the fundamental assumption of the Thin Airfoil Theory, it is simply a statement that the camber line is a streamline of the flow. The theory further assumes that the vortex sheet is located at the chord line since the airfoil is thin. The vortex strength can be calculated by integrating the variation of the vortex sheet from the leading edge to the trailing edge. The Thin Airfoil Theory yields the following solution for the vortex sheet distribution along the camber line, [23]

$$\gamma(\theta) = 2\alpha V_\infty \frac{(1+\cos(\theta))}{\sin(\theta)} \tag{22}$$

and the vortex strength in polar coordinates can be expressed as,

$$\Gamma_0 = \frac{c}{2}\int_0^\pi \gamma(\theta)\sin(\theta)d\theta \tag{23}$$

Substituting Eq. (22) into Eq. (23) and integrating, the circulation is

$$\Gamma_0 = \alpha c V_\infty \int_0^\pi (1+\cos(\theta)d\theta = \pi\alpha c V_\infty \tag{24}$$

Then, the Vortex strength is a function of the angle of attack, chord length, and free stream velocity. This result is valid only for thin and symmetric airfoils, and for two dimensional low speeds (incompressible) flows.

Experiments show that the circulation of each vortex is anywhere between 40% and 60 % of the initial vortex strength and remains constant farther downstream.[24] During the vortex surface interaction the circulation will be considerably reduced once more. For simulation purposes, the circulation of each vortex will be defined as 45 % of the initial vortex strength. The significant reduction on the vortex strength can be considered as a safety factor to ensure that there is a significant three-dimensional surface deformation generated by the vortex pair.

2.5. SUMMARY

The expressions used to estimate the magnitude of the Froude number for the experimental set up can be summarized as,

Froude number,

$$Fr = V_0 / \sqrt{g b_0} \tag{25}$$

Net Induced Velocity,

$$V_o = \frac{\Gamma}{2\pi b_o} \tag{26}$$

Vortex Strength,

$$\Gamma = 0.45 * \pi \alpha c V_\infty \tag{27}$$

Assumptions,

- Concentrated vorticity, point vortex
- Inviscid flow
- Thin Airfoil Theory applies
- Symmetric Airfoils.
- 2-D flows
- Low speed incompressible flows

2.6. ANALYSIS

According to the simulation of the experimental set up, there is an exponential relationship between the vortex separation (b_o) and the Froude number (Fr) , Fig. 25. The net induced velocity is strongly dependent on the vortex separation b_o, Fig. 26. The vortex generator might appear to just meet the main design criteria (Fr=0.15); however, the different parameters involved in the simulation have been underestimated. As a result, the vortex pair for slightly different test parameters still represents a feasible solution. The final test is the observation of the surface deformations during the experiments. Table II depicts the general behavior and trend of different testing parameters.

3. QUALITATIVE TEST PROCEDURE

3.1. FLEXIBILITY

The experimental set up is very flexible. The displacement of the counter rotating vortices toward the surface is due to the net induced vortex velocity, which is mainly a function of D_o, b_o, and α_o.

There is a large domain in which the distance from the free surface, vortex separation, and angle of attack can be varied. However, in order to achieve a Froude number of 0.15, a series of constraints imposed in the experimental set up have to be taken into account. The length of the free surface water tunnel is only 60``, the maximum allowable free stream velocity is 5 in./s., and vortex breakdown is possible according to previous experimental observations if the ratio D_o/b_o is greater than 4.[3]

A feasible range of solutions is given by a wing separation greater than 0.5 in. and less than 0.70 in., and a velocity greater than 3 in/s. and less than 5 in/s. Due to the long wave instabilities the maximum allowable depth for the model is 3.5 in.

3.2. PRELIMINARY SETTINGS

The water tunnel is filled with fresh water to a convenient level, and then the water is filtered with the on-line filtering system available at the facility. The water is filtered in order to remove any type of impurities in the water. According to the type of test, the pressurized dye reservoirs are filled with the appropriate type of dye. After the removal of trapped air, the water tunnel is set to the required testing speed. After a

sufficient waiting period the velocity of the water tunnel will reach a steady state, and the water disturbances due to external sources will dissipate. At this time, qualitative as well as quantitative data can be recorded.

3.3. TEST PROCEDURE

Qualitative data will be recorded at seven different locations. Four locations correspond to different vertical cross sectional areas located at 0.5 ft., 1 ft., 2 ft., and 3.5 ft. from the alpha shaft. The other three correspond to different horizontal cross sections located at the first, second, and third set of 20 in. from the alpha plate, Fig. 28.

A 35mm camera, and a video camera are used to record still and real time motion respectively. The video camera is able to record 30 frames per second, which for the moment is sufficient. Initially, photographs and videotape with several configurations of lightning, shutter speed, type of film, and camera location were recorded to determine the best configuration. Kodak film with ASA 400 is used whenever the laser light is used, and Kodak with ASA 200 whenever standard high intensity photography light is used. A normal shutter speed is around 1/30 of a second, and 1/500 for the 35mm camera and videotape respectively. A faster shutter speed underexposed the pathlines, while at slower shutter speed the pathlines overlapped to the extreme that the vortex motion was indistinguishable. A faster shutter speed in the video camera resulted in a darker, less defined video.

Fluorescent dye in conjunction with a pair of black lights located on the upper part of the tunnel are used to delineate the vortex structure and motion. The cross

sectional areas are visualized using a laser sheet capable of traversing along the test section of the tunnel, Fig. 29.

4. SURFACE TENSION EFFECTS

The mathematical simulation showed the wave pattern is not strongly dependent on the surface tension. A preliminary experiment was designed to investigate the results. The preliminary experimental results also showed the wave pattern was not strongly dependent on the surface tension.

Standing waves were generated at the open test section of the water tunnel. The wave pattern was parallel to the flow direction. The waves were generated with a home made wave maker located in the upstream segment of the test section of the tunnel.

Once the standing waves were generated throughout the free surface, the surface tension of a designated free surface sector was varied by adding different surface contaminants such as motor oil, Fig. 29. The results showed the wave pattern was not significantly affected by surface tension variations. Additional testing is necessary in order to have a final conclusion.

CHAPTER IV.

MEASUREMENTS

1. OBJECTIVE

Local surface deformations and velocity field at and near the surface are needed for the understanding of many free surface flow phenomena such as vortex / wake and free surface interactions. Instantaneous an accurate surface topography information can be used for the development and verification of CFD simulations, as boundary conditions for numerical prediction techniques, and as a medium to identify the physical nature of Synthetic Aperture Radar (SAR) images.

2. QUALITATIVE MEASUREMENTS AND OBSERVATIONS

Several hours of videotape were recorded during the course of the experiments. Different parameters were used in order to confirm the behavior of the vortex pair, and the characteristics of the surface signature. At the same time, the testing parameters were being optimized. The optimization criteria was based on the maximization of the three-dimensional surface signature, and the minimization of unwanted surface disturbances. Table III shows some of the parameters adopted during the experiments. A short videotape which summarizes and describes an experimental test and objectives is available.

2.1. VORTEX PAIR DEVELOPMENT, VORTEX VORTEX INTERACTION

The complexity of the structure and interaction of the vortex couple increases as they move toward the free-surface in the open test section of the tunnel. Figure 30 shows the structure of the vortex couple at different cross sectional areas along the test section. Initially, the vortices have a fine coherent structure. However, as the net induced velocity translates the vortex pair to the free surface, the fine coherent structure is disrupted, new vorticity is generated, and a significant three-dimensional surface signature is created. The vortex bounces from the free surface as shown in Fig. 30c. The flow field near the surface is turbulent. The same type of behavior is observed for different testing parameters. The time the vortex pair takes to arrive to the free surface is directly proportional to the vortex separation b_0, and inversely proportional to the vortex depth D_0.

2.2. DEVELOPMENT OF SURFACE SIGNATURE, SURFACE VORTEX INTERACTION

The free surface of the water tunnel is divided into three sections of twenty inches each, Fig. 28. There is no evidence of any type of vortex surface interaction or disturbances in the first section, Fig. 31a. The vortex pair rises to the free surface in the second section, Fig. 31b. The surface is initially deformed at the location of the main axis of the vortex couple. Then, the width of the signature increases generating the Striations, which grows about $2b_0$ to $3b_0$ as observed by previous researchers.[3, 4, 5] In

the third section the vortex pair interaction with the free surface is completely developed, Fig. 32a. There is evidence of a three dimensional interaction, generation of Scars, and an increase in the width of the signature. Figure 32b shows the three-dimensional deformations initially generated by the counter rotating vortex. The magnitude of the surface signature is directly proportional to the Froude number. The surface signature generated by the vortex couple has similar characteristics to the surface signature generated by the ALM simulation, Fig. 8, and to the surface signature observed by SAR, Fig. 2. The signature prevails and the width of wake increases with time.

3. INSTRUMENTATION

There is deficiency associated with the instrumentation available to reconstruct the surface signature. Current techniques employ intrusive methods such as capacitance probes, or non-intrusive methods such as ultrasonic probes. The existing techniques required a large number of measurements for a comprehensive and accurate description of a surface flow. As result, the application and effectiveness of the existing measurement techniques are limited. A new and innovative 3-D optical topographic mapping system capable of reconstructing the surface signature is presented in the following sections. Recently, three different investigators reported independently the necessity, interest, and similar approaches in free surface elevation mapping.[25, 26, 27]

PART II: 3-D OPTICAL TOPOGRAPHIC MAPPING

CHAPTER V.

INTRODUCTION

1. BACKGROUND

1.1. FLUID DYNAMICS

The reconstruction of the surface signature generated by a pair of counter rotating vortices is necessary in order to gain a better understanding of the turbulent development of the vortex surface interaction. The surface elevation can be correlated with the near surface flow field. Instantaneous and accurate surface topography information can be used for the development and verification of computational simulations, as boundary conditions for numerical prediction techniques, and as a mean to identify the physical nature of Synthetic Aperture Radar (SAR) images.

1.2. MACHINE VISION SYSTEM

Non-intrusive three-dimensional measurements system are extremely important since they provide effective vision to machines. These systems can be classified into two major methods of reconstruction: point by point, and integral. Integral techniques include interferometry and Moiré topography. Point by point techniques include mechanical tactile probes, optical triangulation, optical focusing, and photogrametry.

Point by Point techniques can be further classified as contact and non-contact methods. The there-dimensional surface signature on this application requires a non-contact rapid reconstruction technique, since probes or similar devices disturb the free surface. Non-contact methods can be further classified as: reflectometric, stereometric, and echonometric techniques. Echomometric systems make use of time-of-flight measurements of an energy pulse reflected from a surface to determine the distance to the surface. Reflectometric systems process one or more images of the object to determine, point by point, surface orientation and thus shape. Stereometric techniques determine surface coordinates from two perspectives views which triangulate a series of points on the surface.

In this laboratory application accuracy, simplicity, and flexibility are important design parameters. Stereomeric techniques provide the fundamental tools necessary to design a promising system capable of reconstructing the signature generated by a submerged body.

2. STATE-OF-THE-ART LITERATURE REVIEW

Recently, the interest in surface vortex interactions has increased significantly. Synthetic Aperture Radar (SAR) images show a particular pattern depicting the trajectory of moving bodies on the ocean surface, Fig. 2. In order to understand the structure and evolution of the surface signature a detailed study is necessary. The flow filed near the surface is turbulent, and the exact temporal structure of the surface

deformations is necessary in order to gain a better understanding of the flow structure and development.

There are several water surface reconstruction techniques which are currently under development. They can be classified as non-contact integral methods. Grant I., Padilla I., and Stewart N.[25] attempted to implement Moiré Techniques to measure water surface elevation. The technique combines Moiré and image processing techniques which can be strobed so that the behavior of the water surface can be described as a series of images of wave elevation to be obtained with a contour interval of some millimeters. The technique has the disadvantage that the contrast of the fringes on the water surface is a function of too many variables, such as the grating spacing, reflection of light at the water surface, the aperture of the observing system, and the degree of collimation of the illuminating beam.

Throughout the years, a series of researchers have been trying to develop an optical measurement technique to measure the water surface slope instead of the free surface elevation. Among the first to apply the concept was Hulburt.[28] The technique is based in the reflection or refraction of light. Basically, a light source is placed below (refraction mode) or above (reflective mode) of the water surface. The reflection or refraction of the spatially linearly-varying intensity of the light source is recorded. The intensity of the light is correlated to the slope of the free surface. The concept has been developed to the extend that two slope components can be measured simultaneously at a point. Dabiri D., Zhang X., and Gharib M.[26] have developed a technique based on the reflective mode of the previous concept. This technique integrates optics, colorimetry,

and uses digital image processing to measure the surface deformation of time evolving flows. This technique has the disadvantages that the slope is a function of the physical properties of the reflected light; therefore, surface conditions might affect the accuracy of the final result. A calibration image is necessary in order to transform colors into slopes. In addition, an initial estimate of the angles of the evolving slopes is necessary in order to select the appropriate optical configuration.

L. M. Smith and D. Britton[28] are currently trying to develop a different approach to measure the water surface deformations. Image data from a stand-alone video camera is recorded looking down into a water tank with a known or previously determined pattern on the bottom surface. By analyzing the refraction-induced distortion resulting from the water depth variations, the surface flow pattern can be determined. One scheme currently in development is based upon phase demodulation of a sinusoidally-varying stripe pattern for wave pattern visualization.

CHAPTER VI.

SYSTEM DESCRIPTION

1. OBJECTIVE

The following optical topographic measurement system has been designed to measure the three-dimensional geometry of any reflective surface. The application was originally intended for measuring the surface of an incompressible flow. This technique can be used as a machine vision system and is believed to be a unique and innovative combination of several structured light vision techniques, devices, and mathematical methods. The complete system will be referred to as "3DOTS", which is acronym for Three-Dimensional Optical Topographic System. At the same time, the basic principle of the reconstruction technique is based on the location of three points or dots in space.

2. BASIC DETAIL OF THE CONCEPT

The 3DOTS applies a triangulation method to the various points on a projected and reflected pattern using the three-dimensional position of the focal points of the passive and active cameras. The active camera (image source) is the camera which generates a pattern by modulating a laser beam into an array from a common focus and projects the image onto the surface. The passive camera (detector) is a digital charge coupled (CCD) camera which records the reflected laser array pattern as an image plane, Fig. 33. The surface is reconstructed by correlating the projected and reflected laser array patterns.

The projection of a grid composed of a large number of points, almost simultaneously, is an efficient method, since data storage requirements are reduced considerably. Even more important is the capability of performing near real time measurements of a of moving surface. Near real time measurements are possible, since the necessary information to reconstruct a surface can be recorded in a short period of time. The main obstacle with a multi-projection system is the matching of corresponding points in the projection and reflection plane. It is a difficult task for a computer since the light intensity patterns are a function of the camera angle, light properties, and surface conditions. However, the correlation of image points can be performed manually, or interactively by an operator. A correlation technique which will increase the accuracy and reduce the difficulty of the matching process is currently under development.

The 3DOTS is a flexible system currently optimized for laboratory applications. Ten different data points are recorded for each projected laser beam: the two dimensional coordinates (P_{Mx}, P_{My}) of the laser beam in the projection plane, the coordinates (R_{Mx}, R_{My}) in the reflection plane, and the three-dimensional coordinates of the focal points corresponding to the projection and reflection plane. Figure 34 depicts the experimental set up, the world coordinate system, and the 2-D image plane coordinate systems during the surface measurements.

3. BASIC HARDWARE DESCRIPTION

The equipment used in the 3DOTS are off-the-shelve components except for the Active Camera and the Relative Displacement Mechanism (RDM) which are customized. However, these devices are made or assembled from standard components. A brief description of the main components of the 3DOTS is presented in the following section.

3.1. ACTIVE CAMERA

The active camera is a device developed for topographic applications. This device projects an array of discrete laser beams outward from a common focus. The source of the beamlet array is a single laser light source. The active camera is capable of varying the beamlet spacing of a maximum array of 128 X 128 beamlets. The spacing and beamlet patterns have to be modified according to the nature of the surface and required resolution. The hardware and operations related to this camera are registered in the United States Patent files with a patent number 4,523,809 dated June 18, 1985.[29] Figure 35.

3.2. PASSIVE CAMERA

The reflection of the laser beam array is recorded by one or more high speed, high precision image sensing CCD cameras. Multiple cameras may be used to obtain different perspectives and to eliminate any type of blockage. The resolution of the surface reconstruction is directly proportional to the resolution of the CCD camera.

The passive camera generates a numerical image of the scene, which is then stored in digital form for further processing. The camera which can be used in 3DOTS is the Panasonic GP-MF552 which is vibration resistance, and it has a shutter speed ranging from 1/125 to 1/10000 of a second. This camera is also compact and lightweight. Figure 36.

3.3. RELATIVE DISPLACEMENT MECHANISM

The Relative Displacement Mechanism (RDM) locates the active and passive camera in space. The coordinates of the cameras are necessary in order to calculate the three-dimensional coordinates of the focal points. The coordinate system is centered on the passive camera or primary detector lens.

CHAPTER VII.

CONCEPT DEVELOPMENT

The 3DOTS has the capability to measure three-dimensional surface deformations from two arbitrary perspectives. This system does not require any type of calibration; nevertheless, the location of the cameras in space is necessary in order to locate the corresponding focal points. The two dimensional coordinates of each laser beam are correlated using the principle of similar triangles.

1. MATHEMATICAL MODEL

The technique implemented in the 3DOTS finds the coordinates of the scene from two or more arbitrary perspective views. The law of similar triangles is the mathematical concept incorporated in this technique. The following relationship is obtained with the aid of Fig. 37,

$$\frac{PF_i - PM_i}{PF_j - PM_j} = \frac{PF_i - RS_i}{PF_j - RS_j} \tag{28}$$

During the mapping procedure, the coordinates of the focal points, and the location of the beams in the projection and reflection plane are known. Then, three different equations relating the coordinates of the surface, projection plane and focal point can be generated using Eq. (28), hence,

$$\frac{PF_x - PM_x}{PF_y - PM_y} = \frac{PF_x - RS_x}{PF_y - RS_y} \tag{29a}$$

$$\frac{PF_x - PM_x}{PF_z - PM_z} = \frac{PF_x - RS_x}{PF_z - RS_z} \tag{29b}$$

$$\frac{PF_y - PM_y}{PF_z - PM_z} = \frac{PF_y - RS_y}{PF_z - RS_z} \tag{29c}$$

Equation (29) represents a system of three equations with three unknowns, Rs_X, Rs_Y, and Rs_Z. There is an infinite amount of solutions along the line going through the focal point (PF_i), projection plane (PM_i), and surface point (RS_i).

In order to find the coordinates of the scene and a unique solution for the system of equations, a point in the surface is triangulated by recording the reflection of the laser beam from an arbitrary perspective plane in space. Then, three additional relationships similar to Eq. (29) can be generated. The new system of equations will triangulate a unique solution which represents the coordinates in space of the three-dimensional surface,

$$\frac{RF_x - RM_x}{RF_y - RM_y} = \frac{RF_x - RS_x}{RF_y - RS_y} \tag{30a}$$

$$\frac{RF_x - RM_x}{RF_z - RM_z} = \frac{RF_x - RS_x}{RF_z - RS_z} \tag{30b}$$

$$\frac{RF_y - RM_y}{RF_z - RM_z} = \frac{RF_y - RS_y}{RF_z - RS_z} \tag{30c}$$

Equations (29) and (30) represent an overdetermined system of six equations in three unknowns (Rs_X, Rs_Y, and Rs_Z) which can be solved using singular value decomposition (SVD). By rewriting Eqs. (29) and (30) in matrix form,

$$\begin{bmatrix} 1 & -A & 0 \\ 1 & 0 & -B \\ 0 & 1 & -C \\ 1 & -D & 0 \\ 1 & 0 & -E \\ 0 & 1 & -F \end{bmatrix} x \begin{bmatrix} RS_x \\ RS_y \\ RS_z \end{bmatrix} = \begin{bmatrix} PF_x - A*PF_y \\ PF_x - B*PF_z \\ PF_y - C*PF_z \\ RF_x - D*RF_y \\ RF_x - E*RF_z \\ RF_y - F*RF_z \end{bmatrix} \tag{31}$$

where,

$$A = \frac{PF_x - PM_x}{PF_y - PM_y} \qquad D = \frac{RF_x - RM_x}{RF_y - RM_y}$$

$$B = \frac{PF_x - PM_x}{PF_z - PM_z} \qquad E = \frac{RF_x - RM_x}{RF_z - RM_z} \tag{32}$$

$$C = \frac{PF_y - PM_y}{PF_z - PM_z} \qquad F = \frac{RF_y - RM_y}{RF_z - RM_z}$$

2. ANALYSIS

The 3DOTS employs a simple, robust and extremely flexible mapping technique which is also based on a simple and robust mathematical model. The lines in Fig. 37 trace the path of the projection and reflection of a single laser beamlet generated at the active camera. The surface topography can be reconstructed by projecting a laser beam array and capturing the reflection from one or more arbitrary perspectives. The positions of each laser beamlet in the projection and reflection plane are correlated by using Eq. (31).

The final result is an array of three-dimensional coordinates describing the surface. A mathematical expression describing the surface can be found with a standard

curve fitting technique. Then, the expression can be used for further processing depending on the type of application.

During the mapping of the three-dimensional surface deformation generated by a submerged body, a series of surfaces separated by a short time interval will be reconstructed. The time interval can be varied according to the speed of the CCD camera. Standard video cameras are capable of recording 30 frames/second; however, high speed digital video cameras capable of recording 1000 frames/second or more are available. The number of frames necessary to reconstruct the three-dimensional surface is mainly a function of the correlation technique to be implemented. The correlation procedure is used to match the corresponding location of each beamlet on the projection and reflection plane.

3. COMPUTER SIMULATION

3.1. OBJECTIVE

The purpose of the computer code is to simulate the effectiveness and difficulties in measuring the surface signature generated by a submerged moving body with the 3DOTS. This technique requires as input the projected and reflected laser array patterns, and the three-dimensional location of the focal points. The apparatus employed to project the beam pattern is called "the active camera". The active camera is able to project an array of laser beams from a common focus. A CCD camera, which is also referred as "the passive camera", is used to capture the reflected beam pattern.

3.2. ACTIVE CAMERA

The active camera projects a laser array pattern onto a surface. In order to simulate the active camera the user has to input the three dimensional space location of the focal point, the two dimensional space location of the left side corner closest to the line of sight of the image plane, the angular rotation with respect to the x, y, and z axis of the image plane, the width and length of the projection grid, and the laser beam density. The angular rotation with respect to the coordinate system is necessary in order to project the encoded light beams to a specific region in the three dimensional surface.

3.3. PASSIVE CAMERA

The passive camera records the reflection of the laser beam pattern onto an image plane located in the three dimensional space. The passive camera can be located by specifying the angular rotation with respect to the x, y, and z axis of the image plane, and the location of the focal point. The passive camera is simulated as an ideal camera. This means the image plane is infinite and any point reflected by the surface will be recorded by the image plane. In an experimental set up several perspectives are employed to ensure a complete surface reconstruction.

3.4. METHODOLOGY

First of all, the active camera is simulated by calculating the location of each individual light beam in the projection plane. Then, in order to simulate the passive camera the reflection of the encoded light beams onto one or more perspectives planes has to be

calculated. The reflection is a function of surface and light properties. By assuming an intensive diffuse type of reflection, the laser array pattern in the reflection plane can be estimated with a system of equations in which the fundamental derivation is based on the concept of the unit vector as shown in the following section. The surface can be reconstructed once the location of the projected and reflected laser beams on the projection and reflection plane is known.

The patterns in both of the image planes are now available. The next step is to map each encoded laser beam in the projection plane to the corresponding location in the reflection plane. The matching process represents a difficult challenge in an automated system. During the computer simulation the mapping is performed automatically, since the location of the laser beams are initially calculated internally.

3.4.1. Projection of Laser Array Pattern

If there are three collinear points in the space, and the three dimensional location of two of the points and the x, y, or z position of the third point is known the position of the unknown coordinates of the third point in the space can be estimated. Since the points are collinear the direction of the imaginary line going through the points has to be the same, Fig. 37. The unit vector between the two known points provides the direction of the imaginary line. The two unknown coordinates can be found by writing a relationship for the unit vector including the third point.

For simulation purposes a mathematical expression for the three-dimensional surface to be reconstructed is given, and it is a function of x and y. Since the location of the

projection focal point and the coordinates of the laser beams on the projection plane are given, the laser array pattern can be projected to the three-dimensional surface using the unit vector concept. The relationship results in a system of two equations and two unknowns,

$$(\hat{u}^2 - 1)[PM_x - S_x]^2 + \hat{u}^2[PM_y - Sy]^2 + \hat{u}^2[PM_z - S_z]^2 = 0$$
$$(\hat{v}^2 - 1)[PM_y - S_y]^2 + \hat{v}^2[PM_x - S_x]^2 + \hat{v}^2[PM_z - S_z]^2 = 0 \quad (33)$$

where $\hat{u}$ and $\hat{v}$ are the components of the unit vector from PF_i to PM_i. The three collinear points PF_i, PM_i, and S_i trace the path of a laser beam being projected from the passive camera to the three dimensional surface. PF_i is the focal point which is common for all the laser beams in the projection image plane, PM_i is the location of the beam at the projection image plane, and S_i is the location of the beam on the scene. When the beam is observed from an arbitrary perspective, a path is traced from the scatter reflection of the beam to the reflection image plane, and then from the reflection image plane to the focal point in the passive camera, Fig. 37.

3.4.2. Reflection of Laser Array Pattern

The reflection of the encoded light beam array from the scene to a particular perspective can be calculated by first mapping the encoded light beams onto the three-dimensional surface. Once the encoded laser pattern is projected onto a three-dimensional surface, the laser beam pattern in the reflection image plane can be estimated with a set of equations similar to the ones in Eq. (33).

The reflection focal point, the three-dimensional coordinates of the scene, and some information about the reflection image plane is available. Then, using a procedure similar to the one employed to develop Eq. (33) and with the aid of Fig. 37, the following expression is obtained,

$$(\hat{u}^2-1)[RM_x-S_x]^2+\hat{u}^2[RM_y-Sy]^2+\hat{u}^2[RM_z(RM_x,RM_y)-S_z]^2=0$$
$$(\hat{v}^2-1)[RM_y-S_y]^2+\hat{v}^2[RM_x-S_x]^2+\hat{v}^2[RM_z(RM_x,RM_y)-S_z]^2=0 \quad (34)$$

where $\hat{u}$ and $\hat{v}$ are the components of the unit vector from RS_i to PR_i.

Equations (33) and (34) represent a system of non-linear equations. There are two equations in two unknowns. Newton-Rapson Method is successfully implemented during the simulation in order to find the exact solution for the non-linear set of equations.

4. RECONSTRUCTION

Now, the surface can be reconstructed since the projected and reflected laser array patterns are available. Then, using Eq. (31) the surface coordinates can be calculated for each laser beamlet. The reconstructed surface is described by an array of three-dimensional coordinates. Figure 38 illustrates the basic concept implemented in the 3DOTS.

Figure 39 shows a sample output of the simulation which proves that the 3DOTS is effective and reliable. In Fig. 39 a sinusoidal surface is reconstructed using the 3DOTS. The output shows the surface as an array of 3-D points in space.

5. NUMERICAL TECHNIQUES

The system of equations simulating the optical reconstruction technique can be classified in two different groups. First, the overdetermined system of equations expressed by Eq. (31). There are six equation in three unknowns. Singular Value Decomposition is a very powerful technique for dealing with sets of equations or matrices that are either singular or else numerically very close to singular. The solution provided by the SVD technique is a least square solution. The least square error in the solution is extremely small, almost negligible. Second, the system of equations used to simulate the projection and reflection of light rays represent a system of non-linear equations. Equations (33) and (34) can be solved by using a standard Newton-Raphson Method for nonlinear systems. Efficient Singular Value Decomposition and Newton-Raphson Method subroutines were adapted from 1986-92 Numerical Recipes Software zp.

The original and reconstructed surface with a few laser beamlets are displayed with the aid of VOGLE, which is an ordinary graphics learning environment. Figure 39.

CHAPTER VIII.

RESULTS

1. ANALYSIS

The 3DOTS is a unique, efficient, and flexible surface measurement technique for moving surfaces. The technique has been custom designed to reconstruct the surface signature generated by a submerged body. This technique has the advantage to position the passive or CCD camera at any convenient location in space. In addition, there is not a calibration procedure prior to any measurements. However, in the 3DOTS the position of the projection and reflection plane focal points is a necessary input.

The 3DOTS has the advantage that the position of the active and passive camera are independent. This means the laser beam pattern can be projected to the surface of interest from a convenient and optimum location, unlike similar techniques where the projection and reflection plane have to be perpendicular to each other.[30] Placing the active camera does not represent a significant problem. However, placing the passive camera can be a difficult task since the passive camera has to capture the reflection of the laser array pattern. Several complications may arise, due to the fact that there exists the possibility of light obstruction or weak reflection from a specific perspective depending on the physical and optical properties of the surface. Therefore, the flexibility provided by the 3DOTS to place the passive camera at any particular

location represents a significant advantage since the multiple cameras can be easily implemented.

The coordinates of the focal points are the only type of readings or measurements which have to be performed prior to any surface reconstruction. Locating a point in the three-dimensional space can be a tedious assignment. However, in 3DOTS the type of coordinate system and the relative displacement mechanism (RDM) make the placement procedure of the focal points in space easier and faster. The coordinate system is centered on the primary detector lens (CCD camera), and the RDM measures the relative displacement of the active camera with respect to the passive camera or vice-versa. Therefore, the cameras are able to record and project from the optimum perspective, because they have the unique ability and flexibility to move around in space without any constraints, Fig. 34.

The mapping of each laser beam in the projection and reflection plane is a difficult task in a surface with large elevation gradients. In this case, the disturbances or surface gradients are relatively small, so the images can be decoded interactively with a few strategically placed reference points along the surface. The new decoding technique, currently under development, will reduce the difficulty and increase the accuracy of the matching process significantly for any type of surface. The decoding process represents a larger source of error during the surface reconstruction. Hence, this process should be performed as accurate as possible.

The 3DOTS is a unique, and innovative surface reconstruction technique, and the system's flexibility reduces common constraints significantly. However, the decoding of the projection and reflection plane can be a laborious procedure.

2. RESULTS

The simulation proved that the 3DOTS is reliable, accurate, efficient, versatile, and easy to implement. Figure 39 shows a three-dimensional sinusoidal surface reconstructed by 3DOTS. The least square error generated during the topographic mapping is extremely small. However, the simulation finds the exact location of the reflected laser beams on the projection plane. In an actual experiment some error, which can be evaluated, is introduced during the decoding of the projected patterns. This error will affect the accuracy of the three-dimensional coordinates of the surface.

CHAPTER IX.

CONCLUSION

An experimental study of vortex surface interactions has been performed. It was found that higher Froude numbers resulted in stronger surface signatures. The Inviscid Linearized Theory simulated the surface signature generated by a moving submerged body, and the surface signature was found not to be strongly dependent on the surface tension. General features of vortex free surface interactions were found to agree with results reported by previous researchers.

The Preliminary design of the optical topographic mapping technique represents a significant breakthrough. The 3DOTS has been mathematically developed into a unique, flexible, and innovative surface reconstruction technique. Laser projected patterns reduce data storage requirements. This system is not intrusive, and it has the capability to map the topography of moving surfaces. The 3DOTS has the significant advantage to be independent of surface properties and structure. It is this property that makes the 3DOTS a versatile system. Similar techniques under development are directly dependent on surface composition and optical properties.[25, 26, 27]

The 3DOTS may be used to measure surface deformations (instantaneous surface coordinates) which can be converted to velocity information. Such data is unique, and useful towards understanding of vortex surface interactions including validation of numerical and turbulence models. The three-dimensional optical topographic mapping technique can also be the interface with image (signal) processing

for non-acoustic detection efforts. In addition, the 3DOTS has potential machine vision applications since the concept is independent of surface type or conditions. The mathematical method and simulation proved that 3DOTS is a promising and valuable system. Future work is intended in building a working model of this concept and in applying this model to a laboratory experiment.

LIST OF REFERENCES

LIST OF REFERENCES

[1] Lugt, H. J., "Vortex Flow in Nature and Technology,", 1983.

[2] Sarpkaya, T, ``Brief Reviews of Some Time Dependent Flows," *Journal of Fluid Engineering*, Vol. 114, 1992, pp.283-298.

[3] Sarpkaya, T., and Henderson, D. O., Jr., ``Surface Disturbances Due to Trailing Vortices," *Technical Report No. NPS-69-84-004*, 1984, Naval Postgraduate School, Monterey, California.

[4] Sarpkaya, T., ``Surface Signatures of Trailing Vortices and Large Scale Instabilities," *Proceedings of the Colloquium on Vortex Breakdown*, (ed. R.W. Staufenbiel), pp. 145-187, Aachen, Germany, 11-12 February 1985.

[5] Sarpkaya, T., and Henderson, D. O., Jr., ``Free Surface Scars and Striations due to Trailing Vortices Generated by a Submerged Lifting Surface," *AIAA 85-0445*, presented at the 23rd Aerospace Sciences Meeting, Reno, Nevada, 14-17 January 1985.

[6] Sarpkaya, T., and Suthon, P. B. R., ``Interaction of a Vortex Couple with a Free Surface," *Experiments in Fluids*, Vol. 11, 1991, pp. 205-217.

[7] Suthon, P. B. R., ``Interaction of a Vortex Pair with a Free Surface: Measurement and Computations," *AD-A233-045*, M.S. and Engineer Degree Thesis, 1990, Naval Postgraduate School, Monterey California.

[8] Rau, D. H., ``Free Surface Scars and Striations," *AD-A212-429*, M.S. and Engineering Degree Thesis, 1989, Naval Postgraduate School, Monterey California.

[9] Sarpkaya, T, 1992c, ``Three-Dimensional Interactions of Vortices with a Free Surface," *AIAA-92-0059*.

[10] Willmarth, W. W., Tryggvason, G., Hirsa, A., and Yu, D., ``Vortex Pair Generation and Interaction with a Free Surface," *Physics of Fluids*, A-1, Vol. 1, 1989, pp.170-172.

[11] Bernal, L. P. and Kwon, J. T., ``Vortex Ring Dynamics at a Free Surface," *Physics of Fluids*, A, Vol. 1, 1989, pp. 449-451.

[12] Bernal, L. P., Hirsa, A., Kwon, J. T., and Willmarth, W. W., ``On the Interaction of Vortex Rings and Pairs with a Free Surface for Varying Amounts of Surface Active Agent," *Physics of Fluids*, A, Vol. 1, 1989, pp. 2001-2004.

[13] Fish, S., *Physics of Fluids*, A, Vol. 3, 1991, pp. 504-506.

[14] Wu J. M., Vakili A., Wu J.Z., "Oceanographic simulation development Project", Final Report, 1993, UTSI, Tullahoma, Tennessee

[15] Ohring, S. And Lught, H. J., "Interaction of a Viscous Vortex Pair with a Free Surface," *J. Fluid Mech.* 227, 1991, 47-70.

[16] Lugt, H. J. And Ohring, S., " The Oblique Ascent of a Viscous Pair Toward a Free Surface," *J. Fluid Mech.* 236, 1992, 461-476

[17] Tryggvason, G., Yu D." The Free Surface Signature of Unsteady Two-Dimensional Vortex Flows. J. *Fluid Mech.* 218, 1990, 547-572.

[18] Fish, S., "Ambient Free Surface Wave Modification by a Submerged Vortex Pair," Ph.D. Thesis, University of MD, College Park, 1989.

[19] King, B. K., "Time-Domain Analysis of Wave Exciting Forces on Ships and Bodies," Doctoral Dissertation, The University of Michigan, 1987.

[20] Newman, J.N., "Marine Hydrodynamics," MIT Press, Cambridge, MA, 1977.

[21] Milgram, J. H., Peltzer, R. D. and Griffin, O. M.: Suppression of Short Sea Waves in Ship Wakes-- Measurements and Observations (1993). *Submitted for publication.*

[22] Milgram, J. H., Skop, R. A., Peltzer, R. D. and Griffin, O. M.: Modeling short sea wave energy distributions in the far wake of ships (1993). *Submitted for publication.*

[23] Anderson J. D., "Fundamentals of Aerodynamics", McGraw-Hill Book Company, 1984.

[24] Govindaraju, S. P. and Saffman, P. G., Flow in a turbulent Vortex, *The Physic of Fluids*, Vol. 14, No. 10, 1971, pp. 2074-2080.

[25] Grant I., Padilla I., Stewart N.: " Measurement of Water Surface Elevation Using Moiré Techniques," *Proc. of the International Conference on Offshore Mechanics and Arctic Eng. Symposium* v II (of VI), 1989. Publ. by The American Society of Mechanical Engineers (ASME), New York, NY, p 547-552.

[26] Zhang X., Dabiri D., and Gharib M.:" A Real Time Free Surface Elevation Mapping Technique," Submitted to the Seventh International Symposium on Applications of Laser Techniques to Fluid Mechanics. Lisbon, Portugal, July 1995.

[27] Britton Doug, "A Refractive Technique for Free Surface Visualization Using Image Processing", Master Thesis, The University of Tennessee Space Institute. 1994.

[28] Hulburt, *J. Opt. Soc. Am.* 24, 35 (1934).

[29] Taboada J., Altschuler B. R., United States Patent files, Patent # 4,523,809, June 18, 1985.

[30] Altschuler M. D., Bae K., Altschuler B. R., Dijak, Tamburino L. A., Woolford B., "Robot Vision by Encoded Light Beams, "Three-Dimensional Macnine Vision," Takeo Kanade. 1987.

APPENDICES

1. LIST OF FIGURES

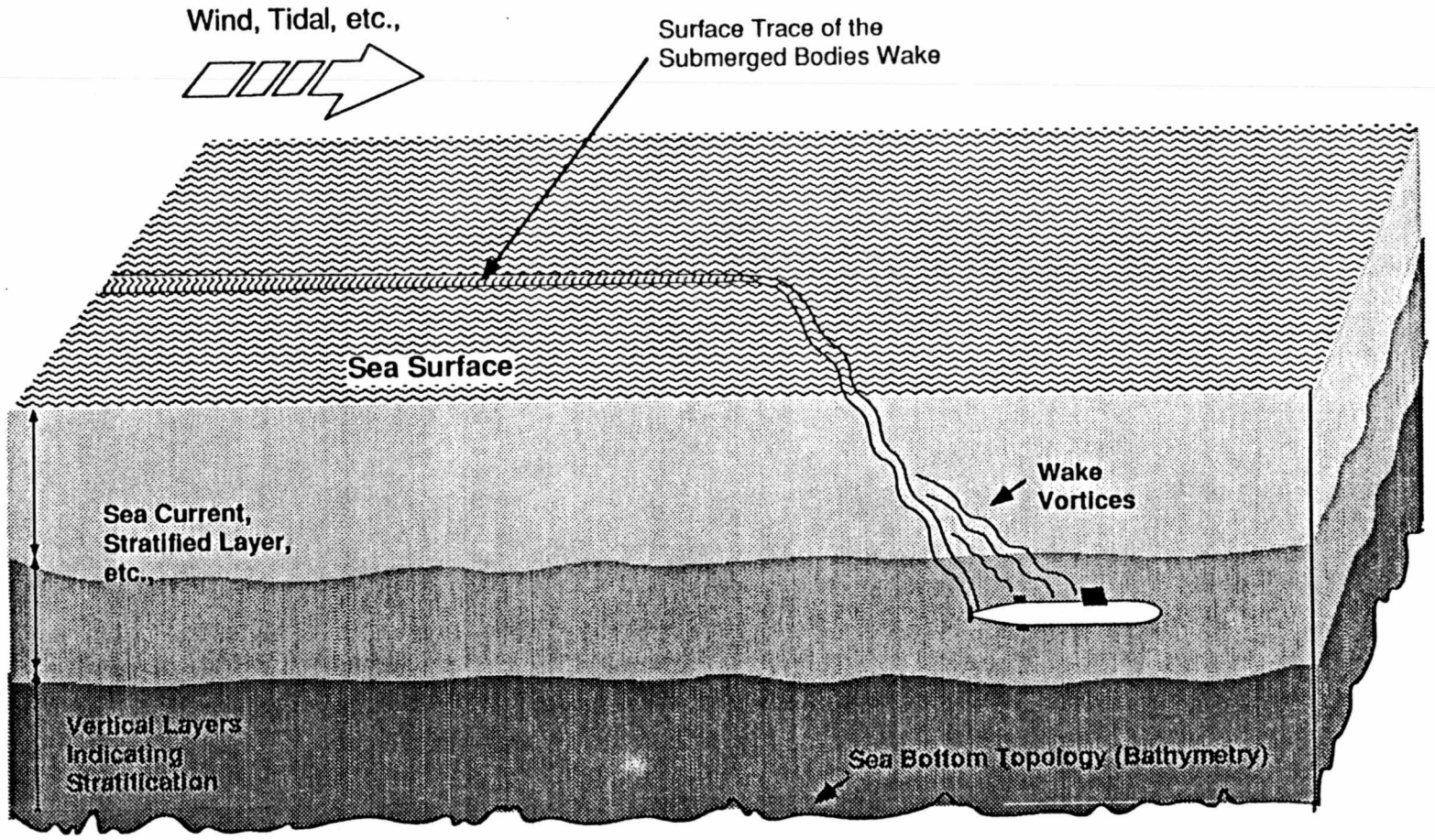

Fig. 1. Signature generated by a submerged body.

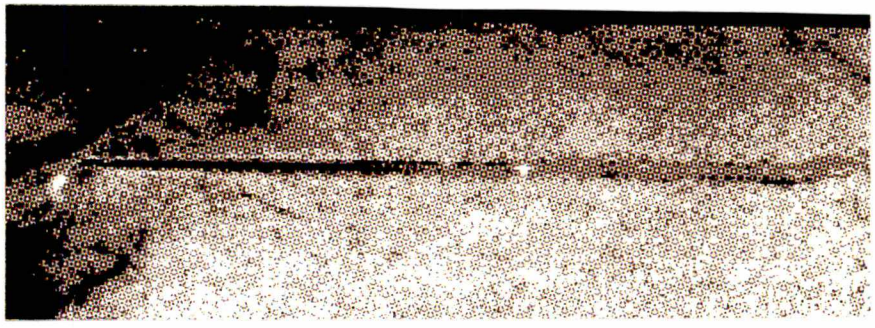

a) SAR image shows approximately four miles of the wake of a naval vessel.
Source: American Scientist, Volume 81, No.1, pp. 19-20 Jan.-Feb. 1993, Publ. Sigma Xi.



b) SAR image shows the surface "signature" generated by a ship.
Source: Sarpkaya, T., and Henderson, D. O., Jr., ``Surface Disturbances Due to Trailing Vortices," *Technical Report No. NPS-69-84-004*, 1984, Naval Postgraduate School, Monterey, California.

Fig. 2. Synthetic Aperture Radar (SAR) images.

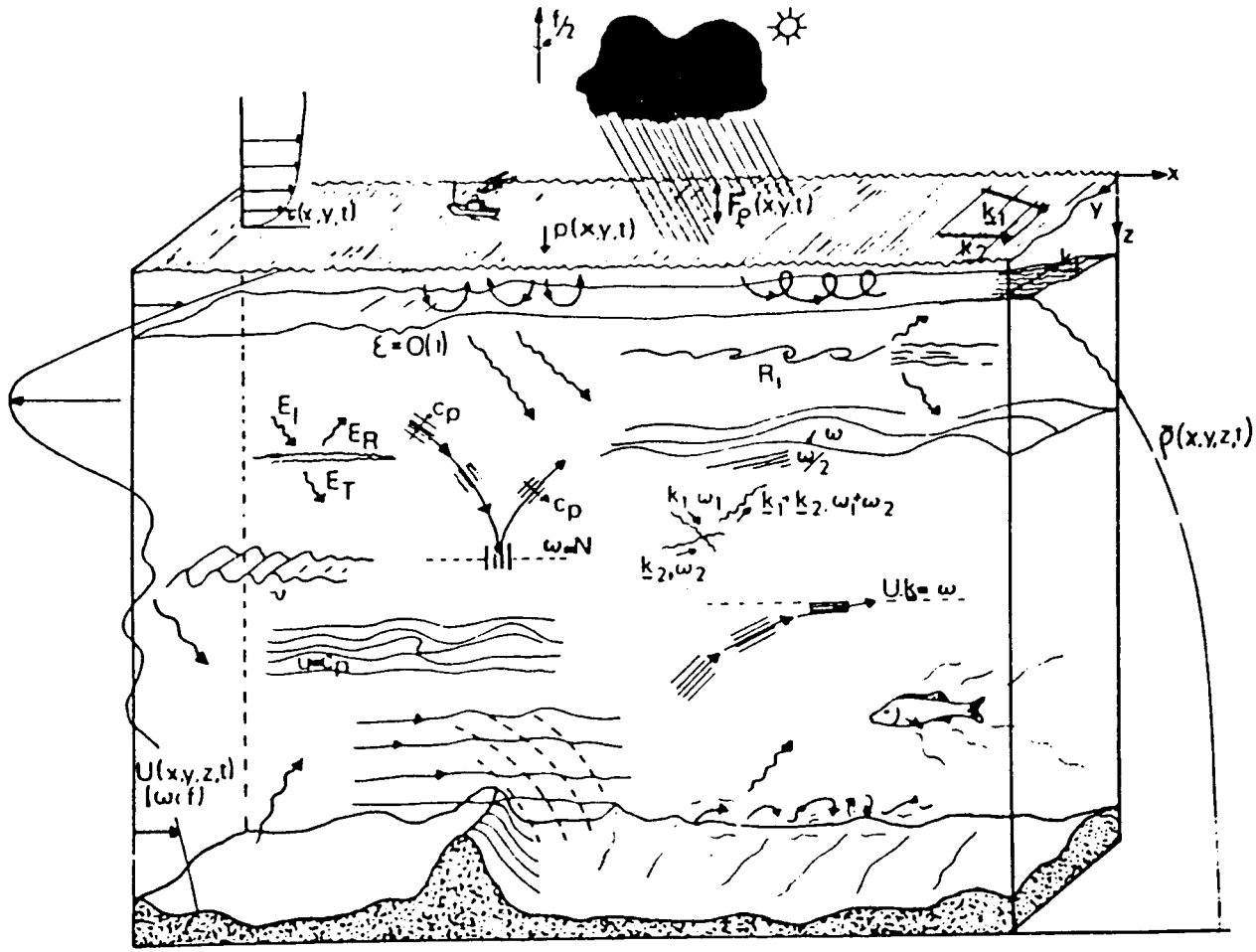

Fig. 3. Pictorial representation of the physical processes involved in the generation, interaction and dissipation of internal waves.

Source: LeBlond and Mysak. "Waves in the Ocean," Elsevier Scientific Publishing Company. 1978.

Submarine Vortices

-Hull Vortices
-Necklace Vortices
-Tip Vortices
-Turtle Back Vortices
-Karman Street
-Flow Over a Cavity

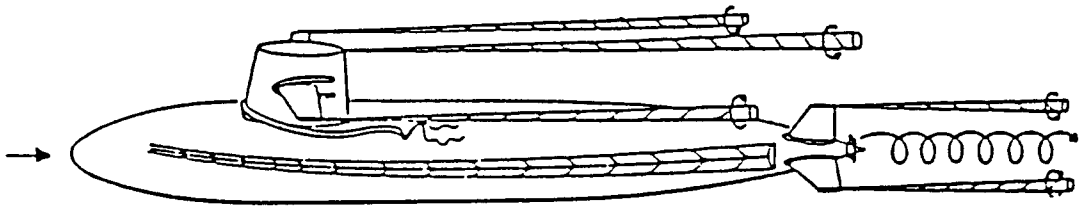

Fig. 4. Vortices generated by a submerged moving body.
Source: Lugt, H. J., "Vortex Flow in Nature and Technology,", 1983.

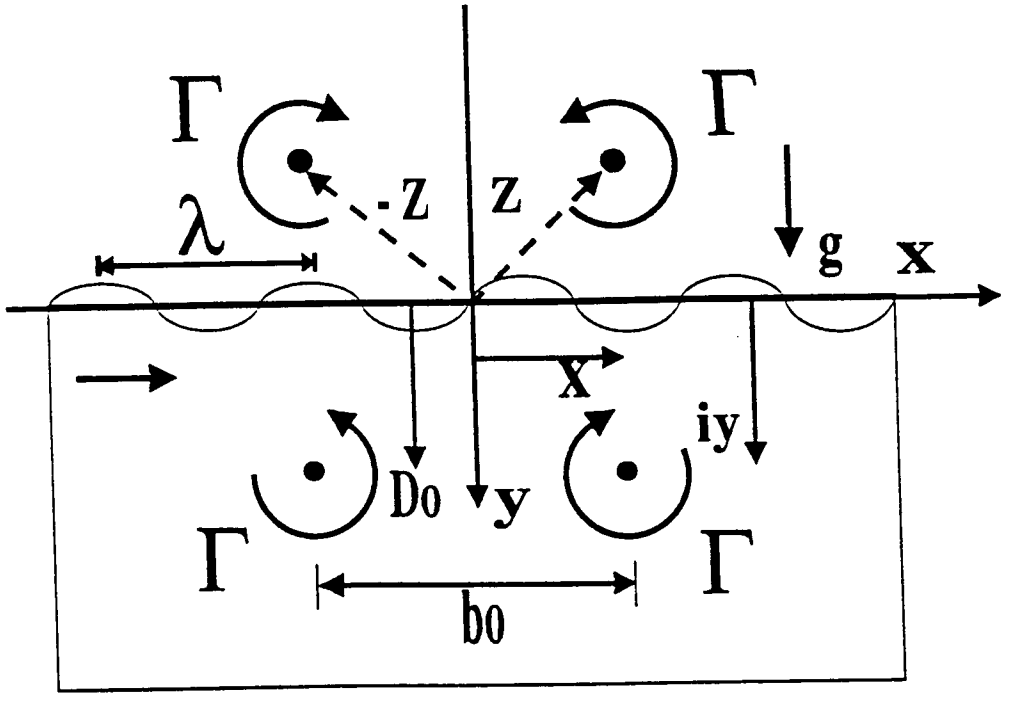

Fig. 5. Simplified model. Basic parameters involved during the experimental and mathematical simulation.

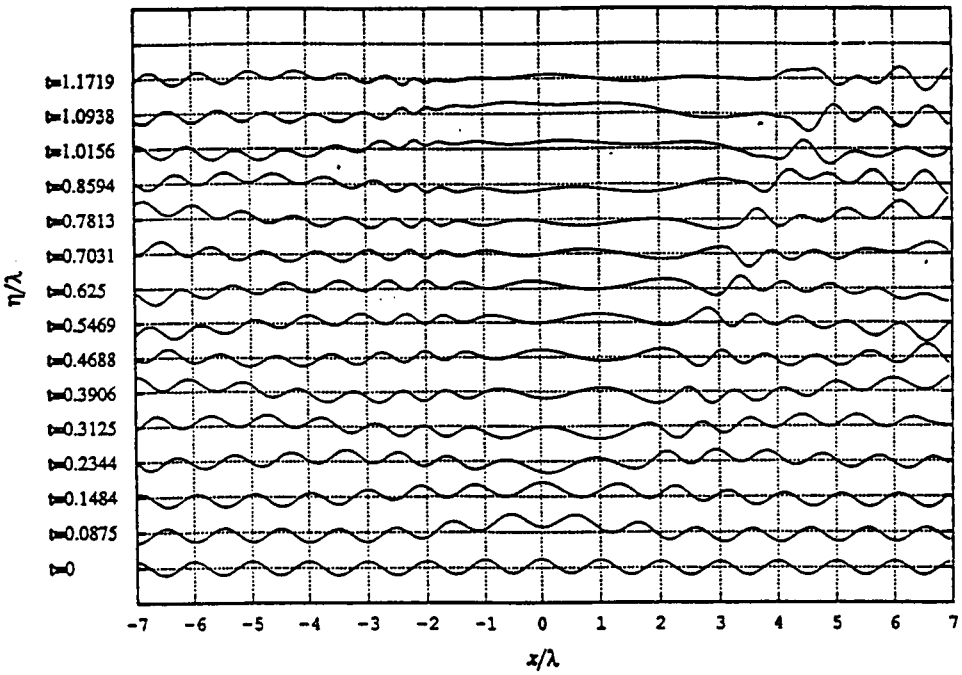

Fig. 6. Counter rotating vortex interaction and surface deformation. Mathematical modeling. (Fr=0.125, S/λ=2.5, D/λ=1.25)

Source: Wu J. M., Vakili A., Wu J.Z., "Oceanographic simulation development Project", Final Report, 1993, UTSI, Tullahoma, Tennessee.

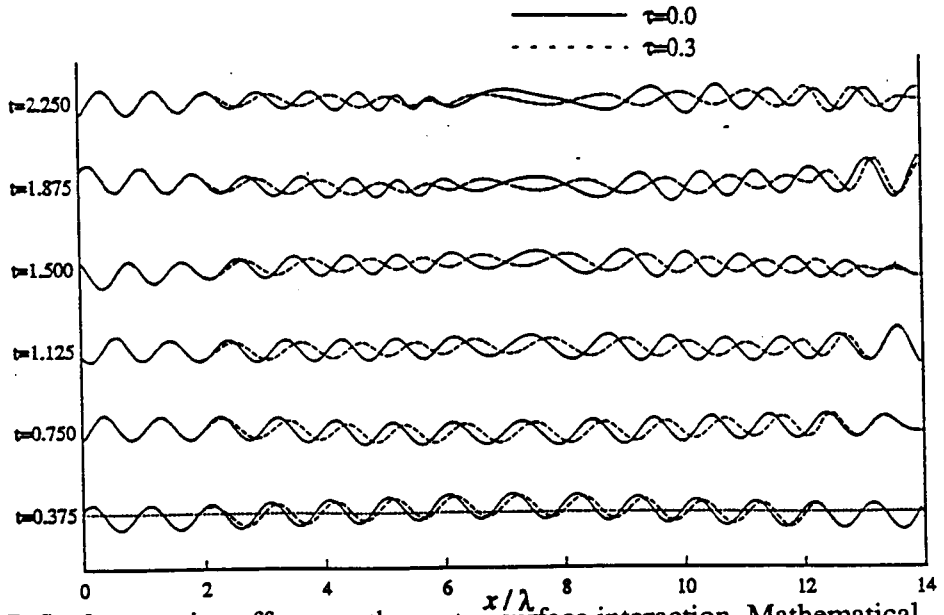

Fig. 7. Surface tension effects on the vortex surface interaction. Mathematical modeling. (Fr=0.3, S/λ=1, D/λ=3, τ=0.3)

Source: Wu J. M., Vakili A., Wu J.Z., "Oceanographic simulation development Project", Final Report, 1993, UTSI, Tullahoma, Tennessee.

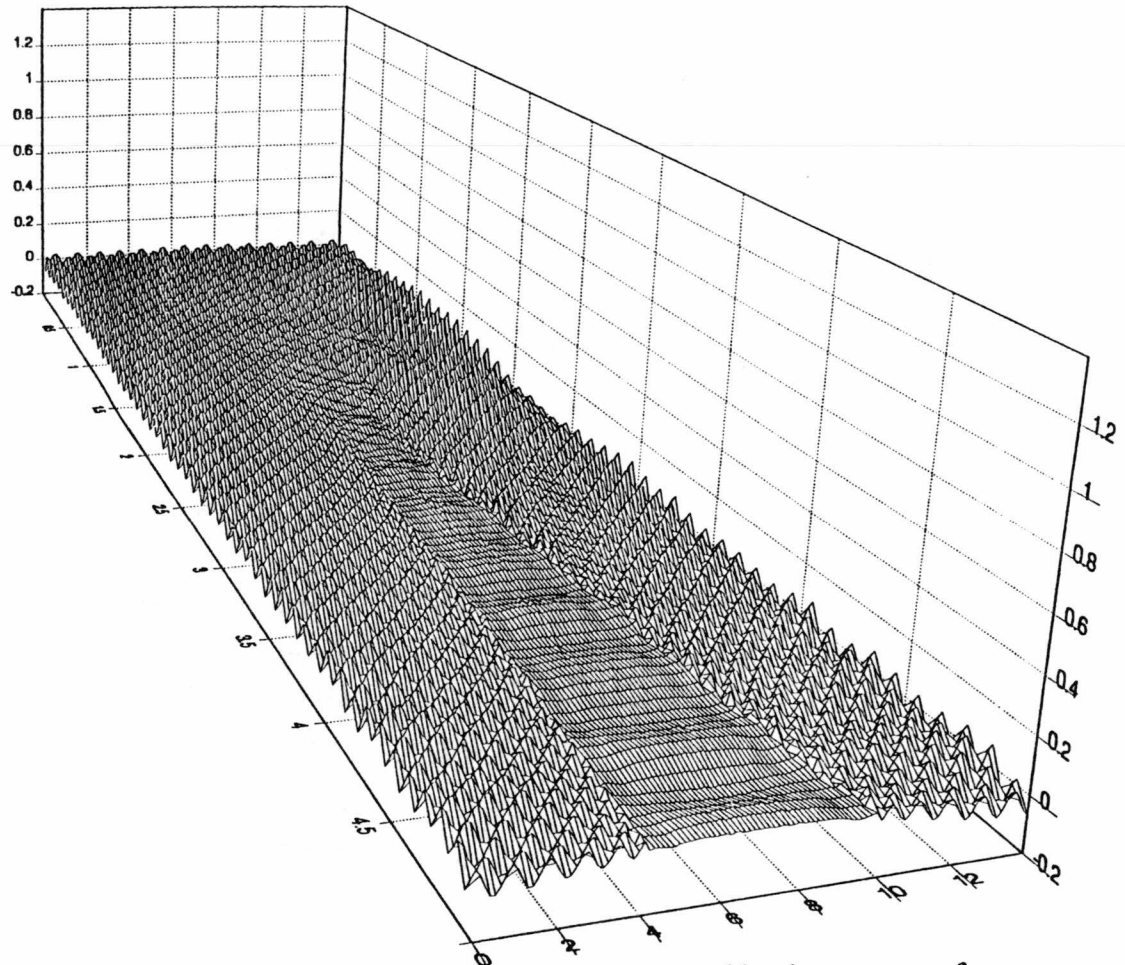

Fig. 8. Three-Dimensional surface signature generated by the vortex surface interaction. (Fr=0.1, S/λ=1, D/λ=3)

Source: Wu J. M., Vakili A., Wu J.Z., "Oceanographic simulation development Project", Final Report, 1993, UTSI, Tullahoma, Tennessee.

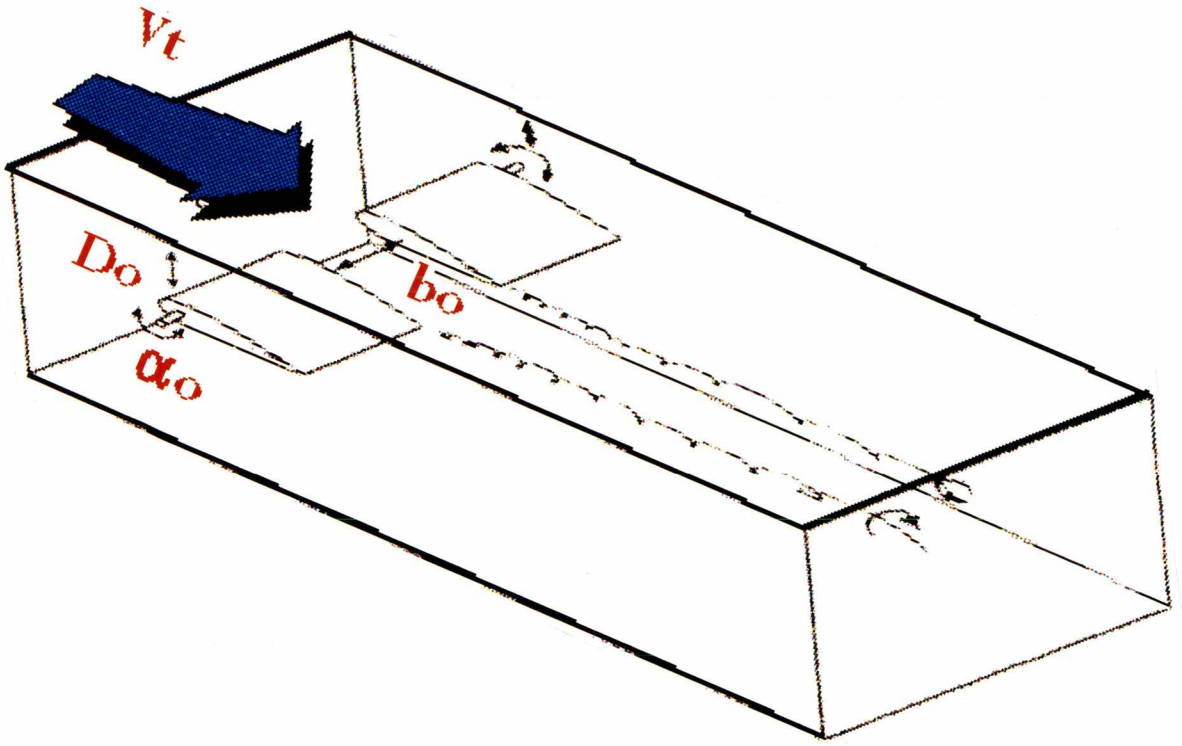

Fig. 9. Experimental set up. Objective is to generate strong vortices in order to produce a 3-D surface signature.

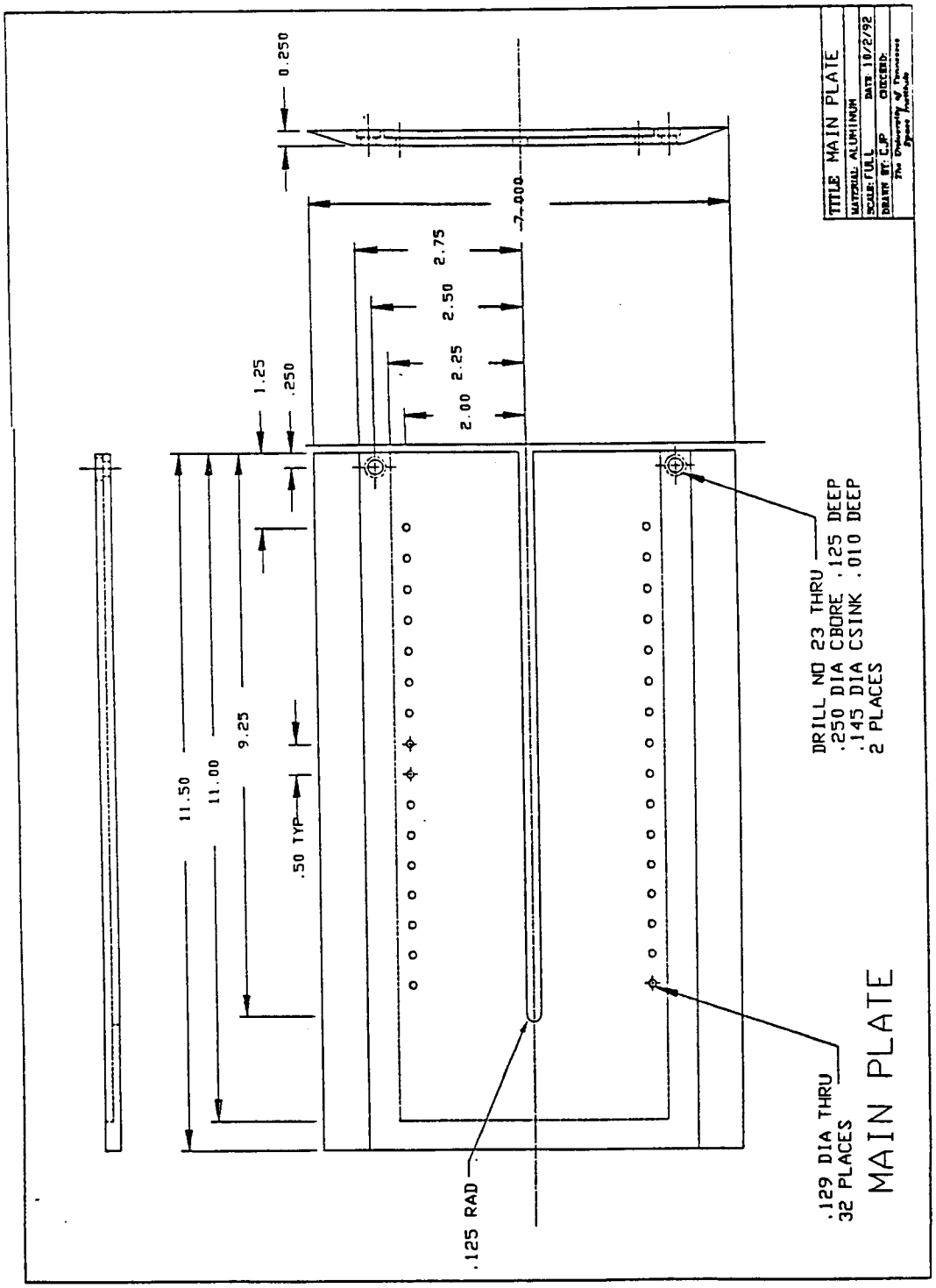

Fig. 10. Experimental set up. Engineering drawings. Mainplate.

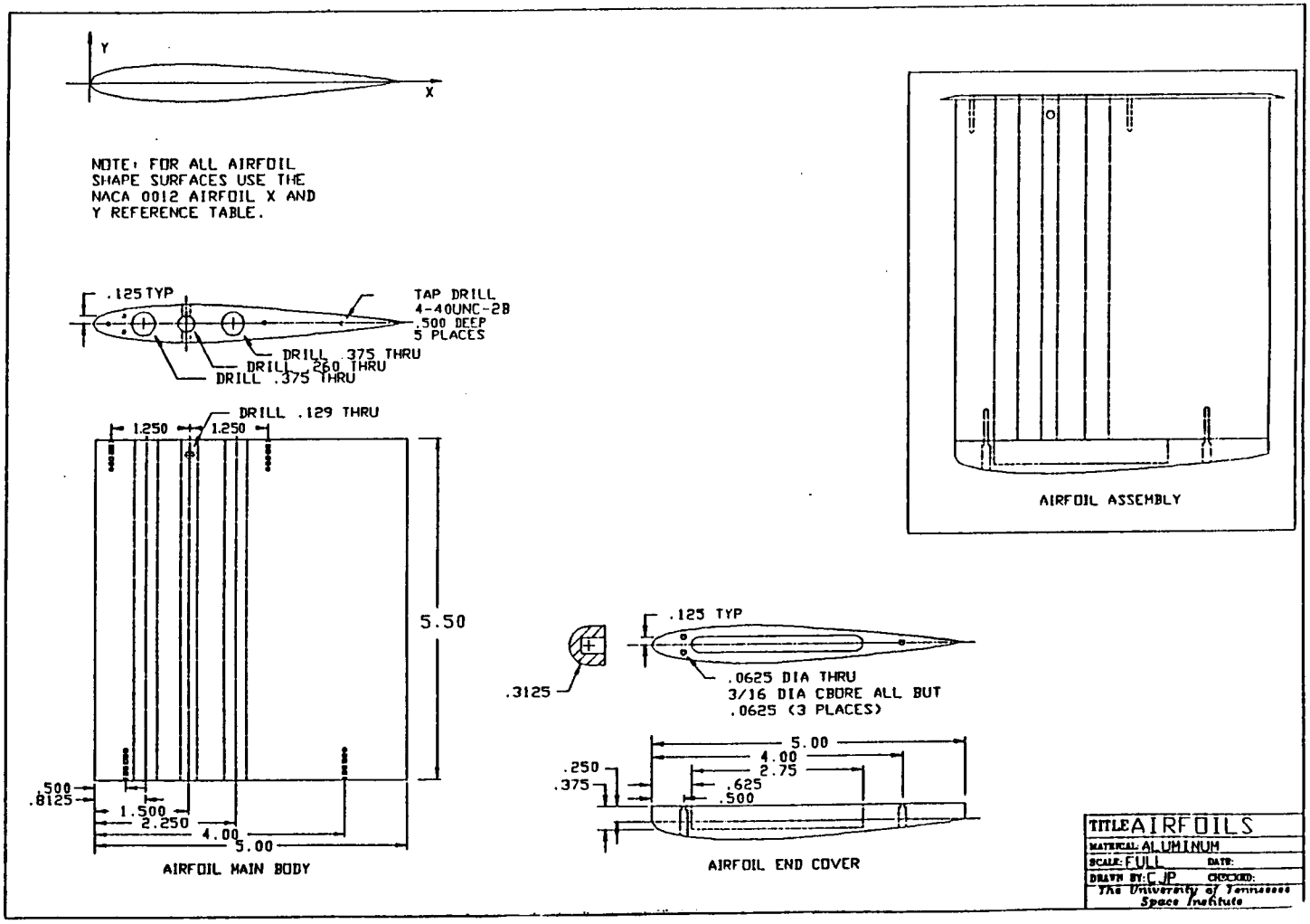

Fig. 11. Experimental set up. Engineering drawings. Wing Section.

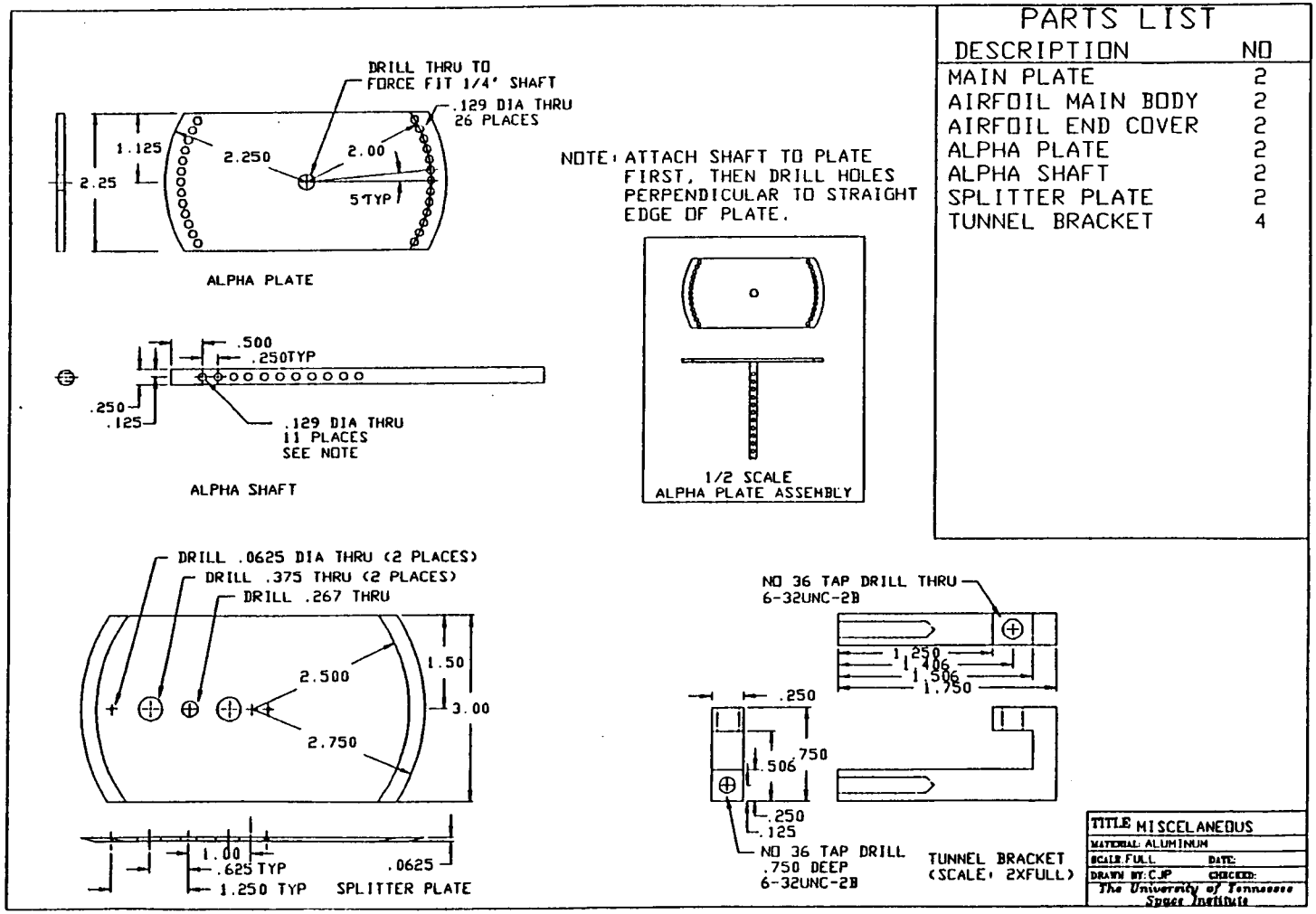

Fig. 12. Experimental set up. Engineering drawings. Miscellaneous.

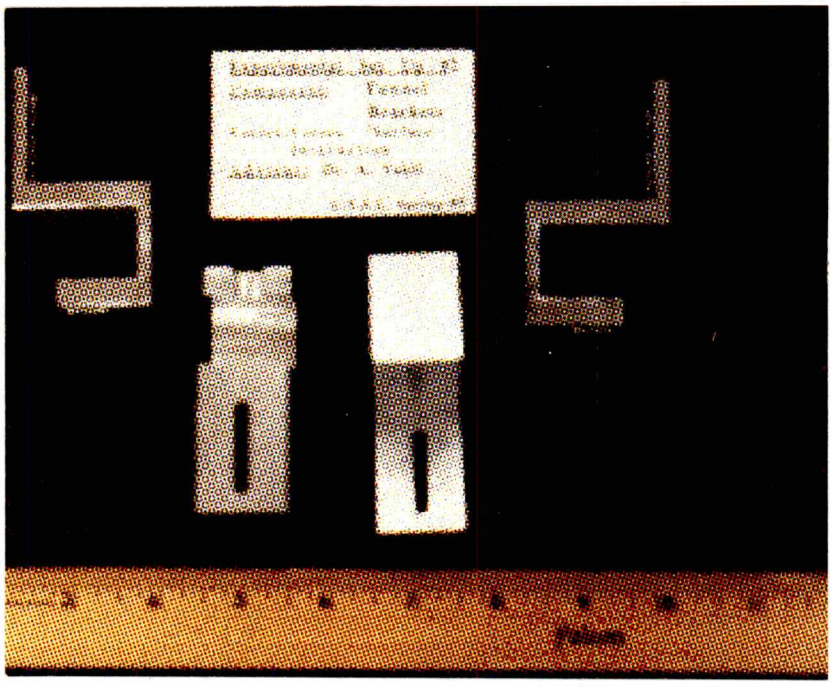

Fig. 13. Tunnel Brackets.

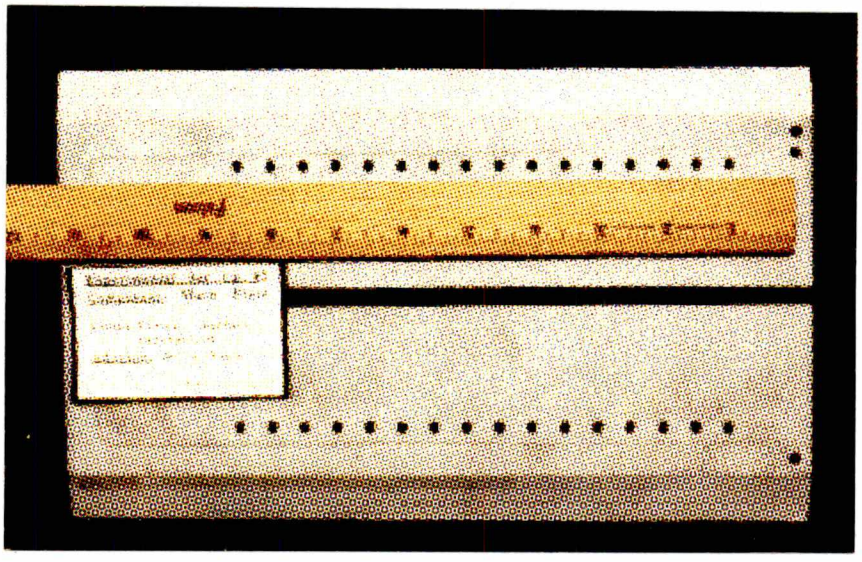

Fig. 14. Main Plate.

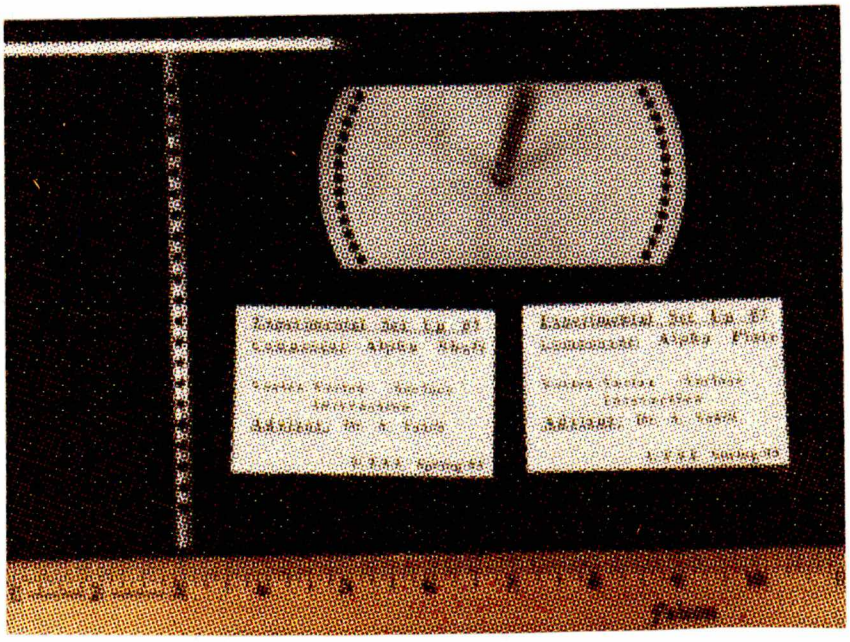

Fig. 15. Alpha Plate and Alpha Shaft.

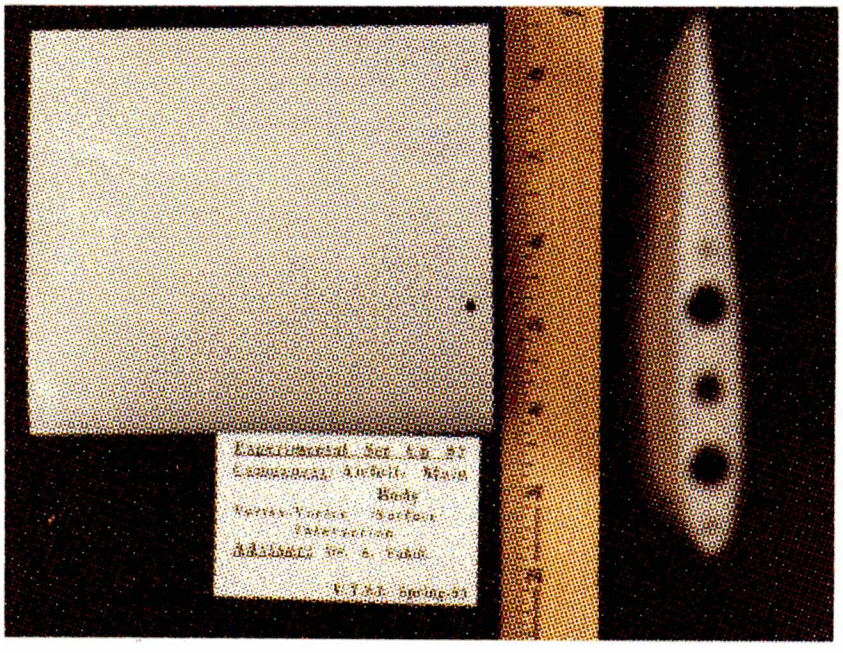

Fig. 16. Wing Section Main Body.

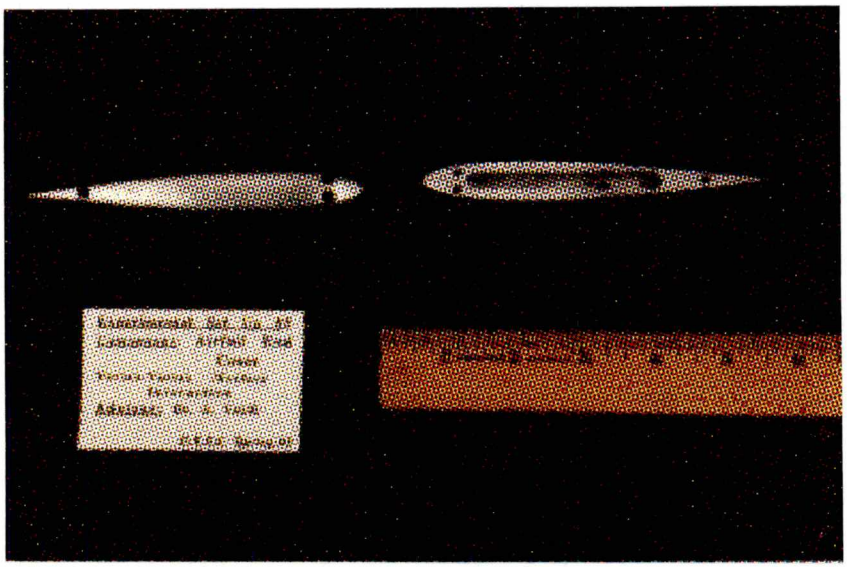

Fig. 17. Wing Section End Cover.



Fig. 18. Splitter Plates.

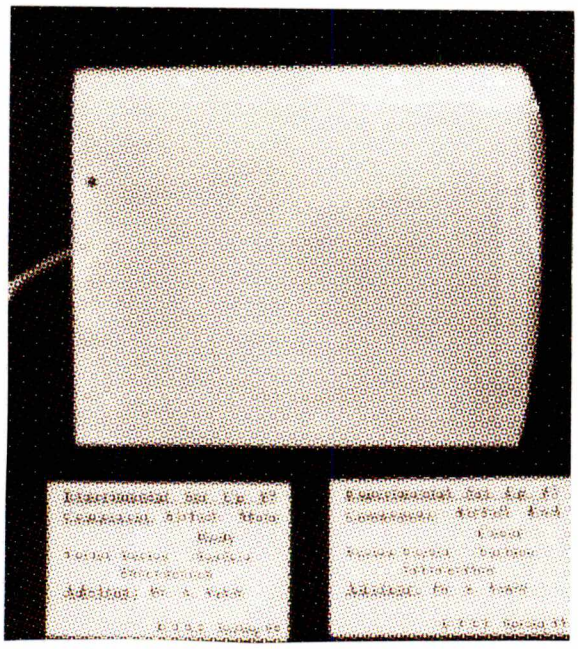

Fig. 19. Wing Section End Cover, Wing Section Main Body, and Dye Injector Tubes.

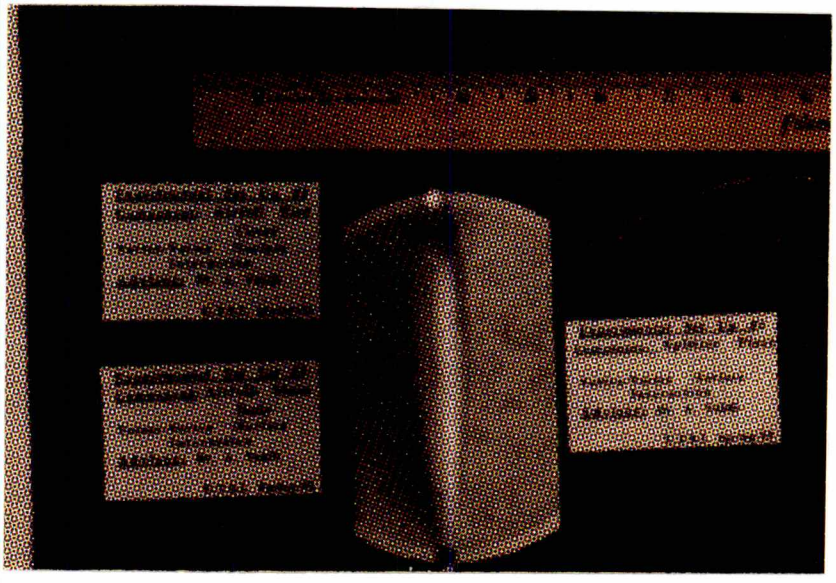

Fig. 20. Wing Section End Cover, Wing Section Main Body, Spliter Plate, and Dye Injector Tubes.

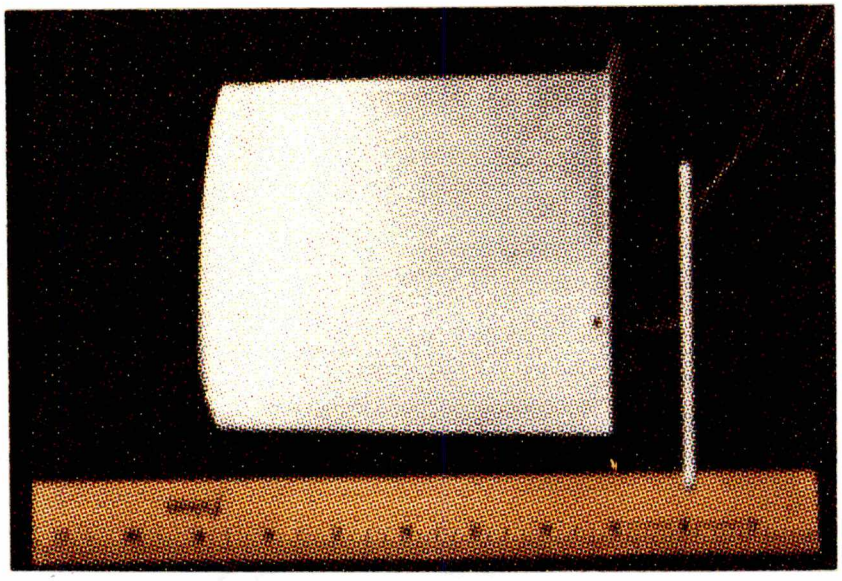

Fig. 21. Alpha Plate, Alpha Shaft, Wing Section Main Body, Wing Section End Cover, Splitter Plate, and Dye Injector Tube.

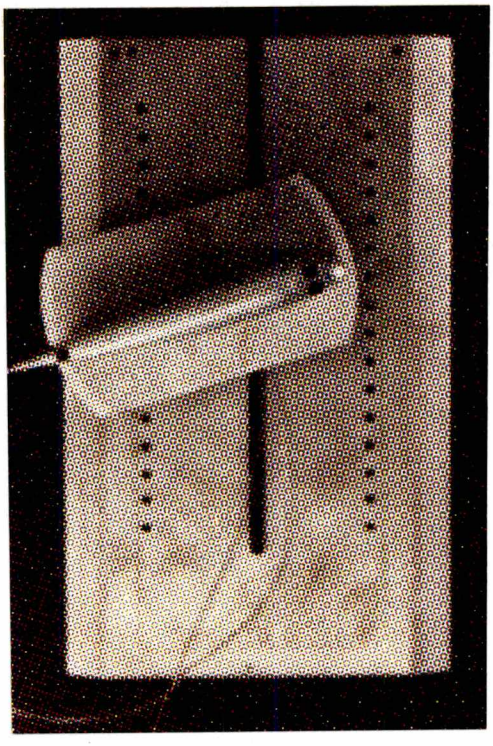

Fig. 22. Main Plate, Alpha Plate, Alpha Shaft, Wing Section Main Body, Wing Section End Cover, Splitter Plate, and Dye Injector Tube.

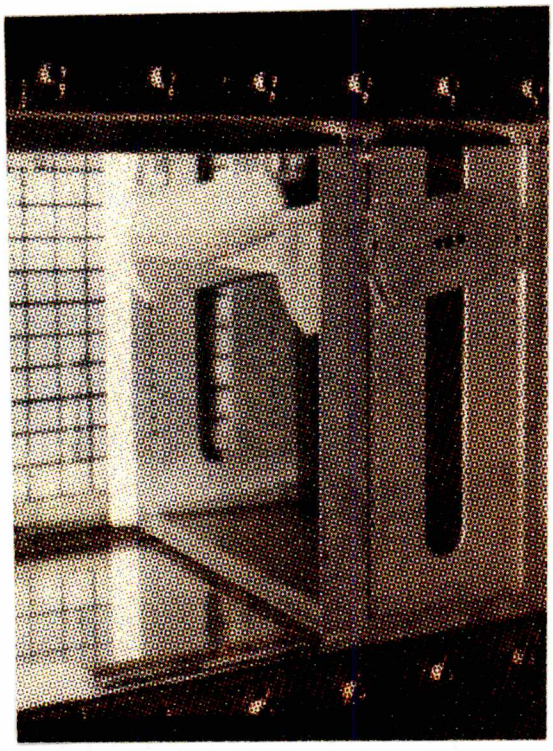

a) Side view.

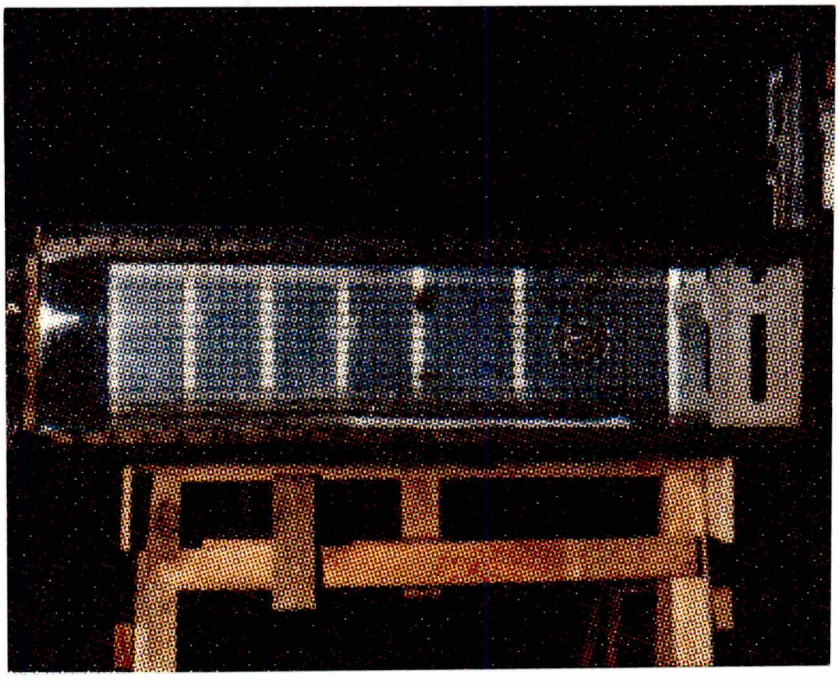

b) Side view test section.

Fig. 23. Experimental set up installed at the test section. Different perspectives.

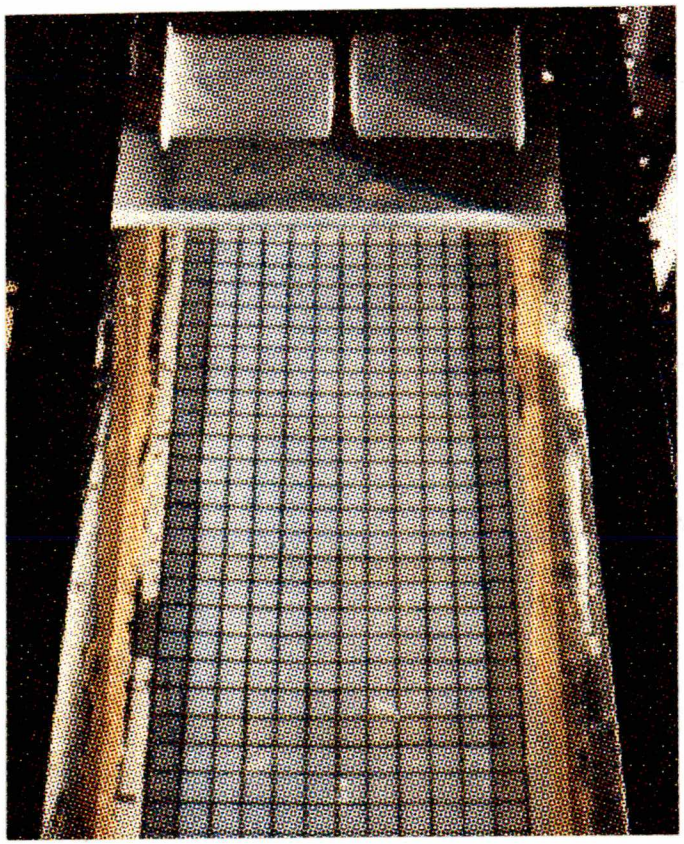

c) Top view test section.

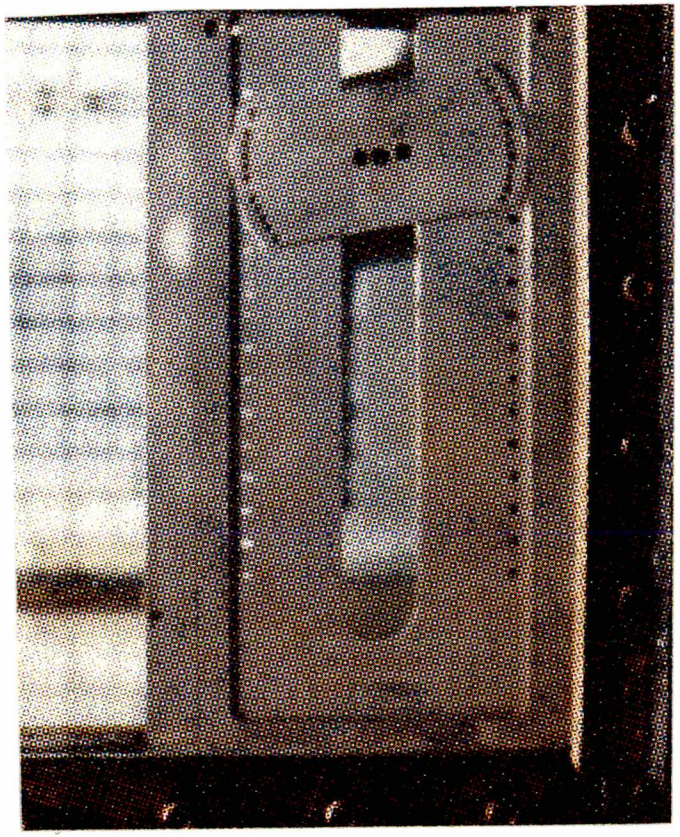

d) Side view.

Fig. 23. (continued).

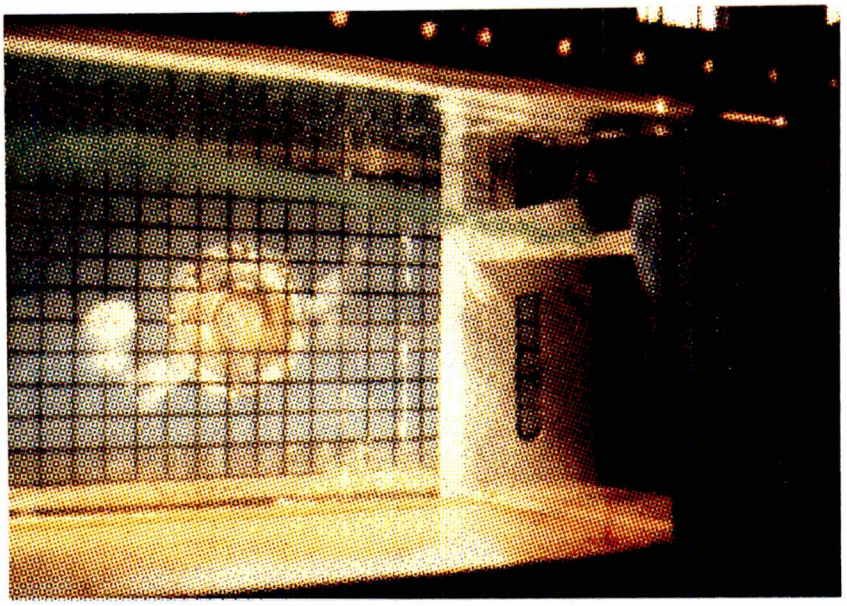

a) Side view. Wing tip vortex.

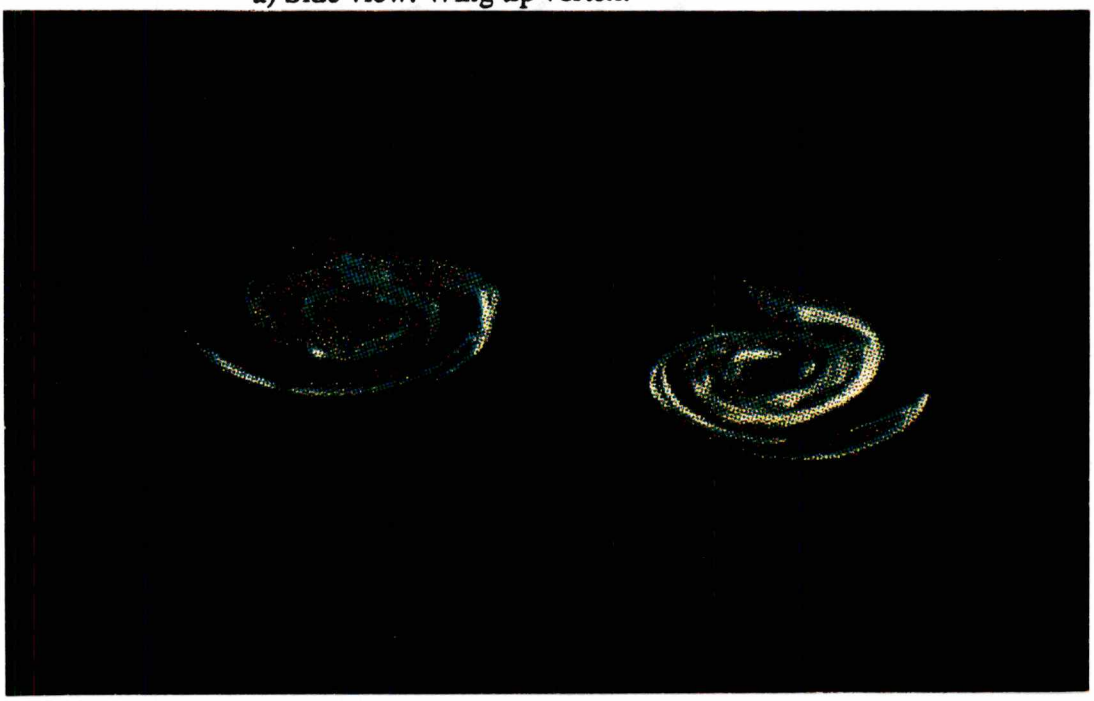

b) Cross section transverse to vortex axis.

Fig. 24. Counter rotating vortices generated by the experimental model.

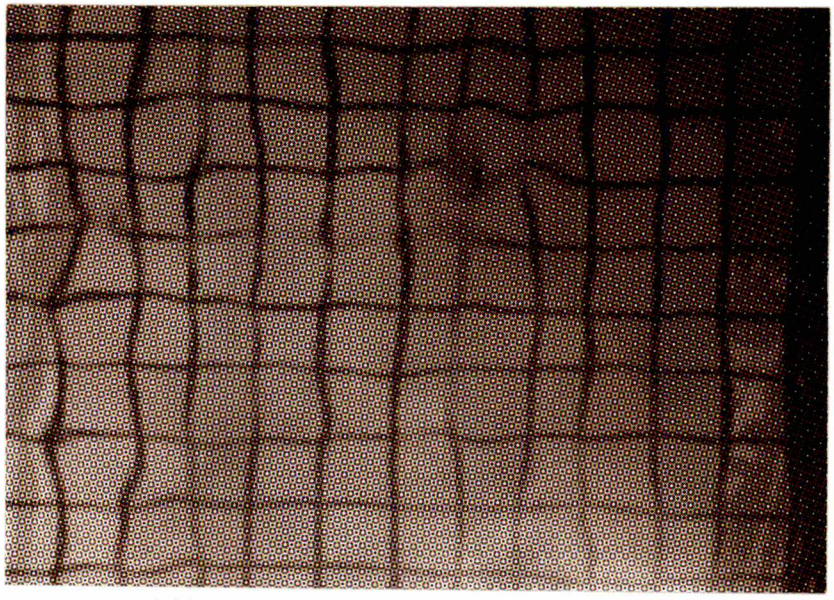

c) Vortex couple arrives to the free surface.

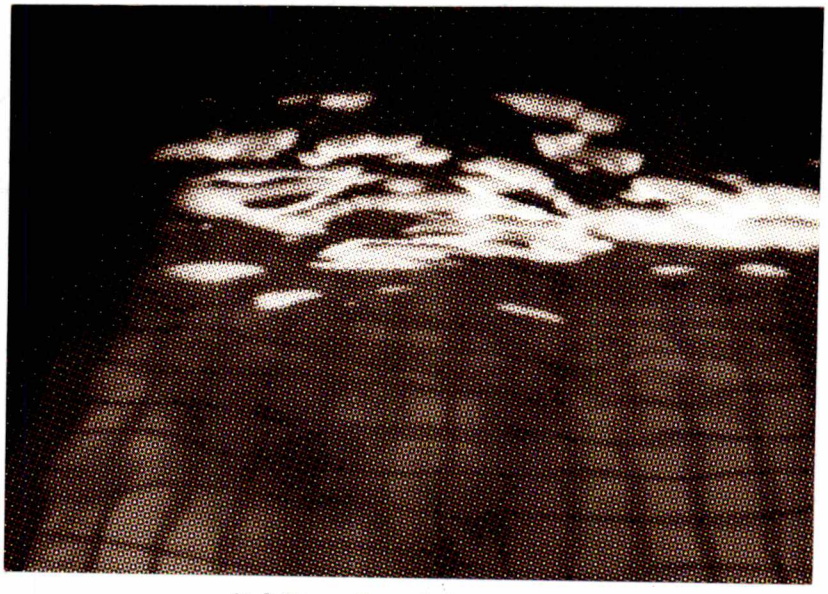

d) 3-D surface deformations.

Fig. 24. (continued).

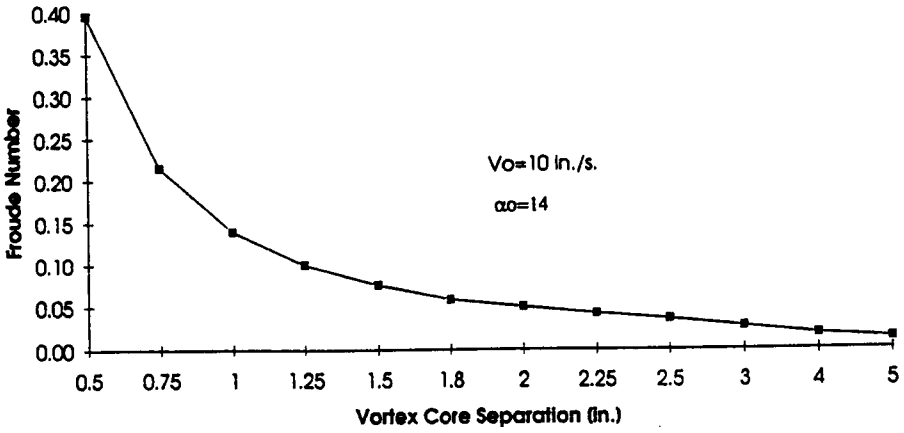

Fig. 25. Vortex core separation Vs. Froude Number.

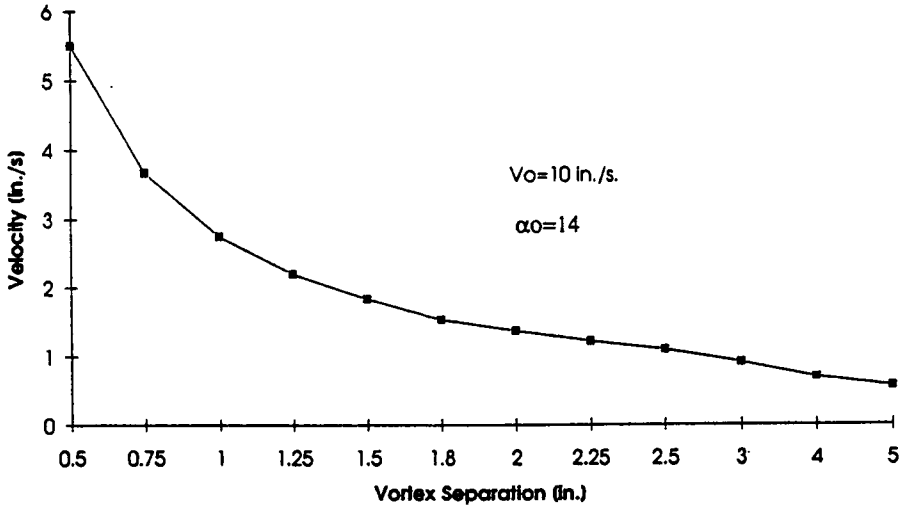

Fig. 26. Vortex core separation Vs. Induced Velocity.

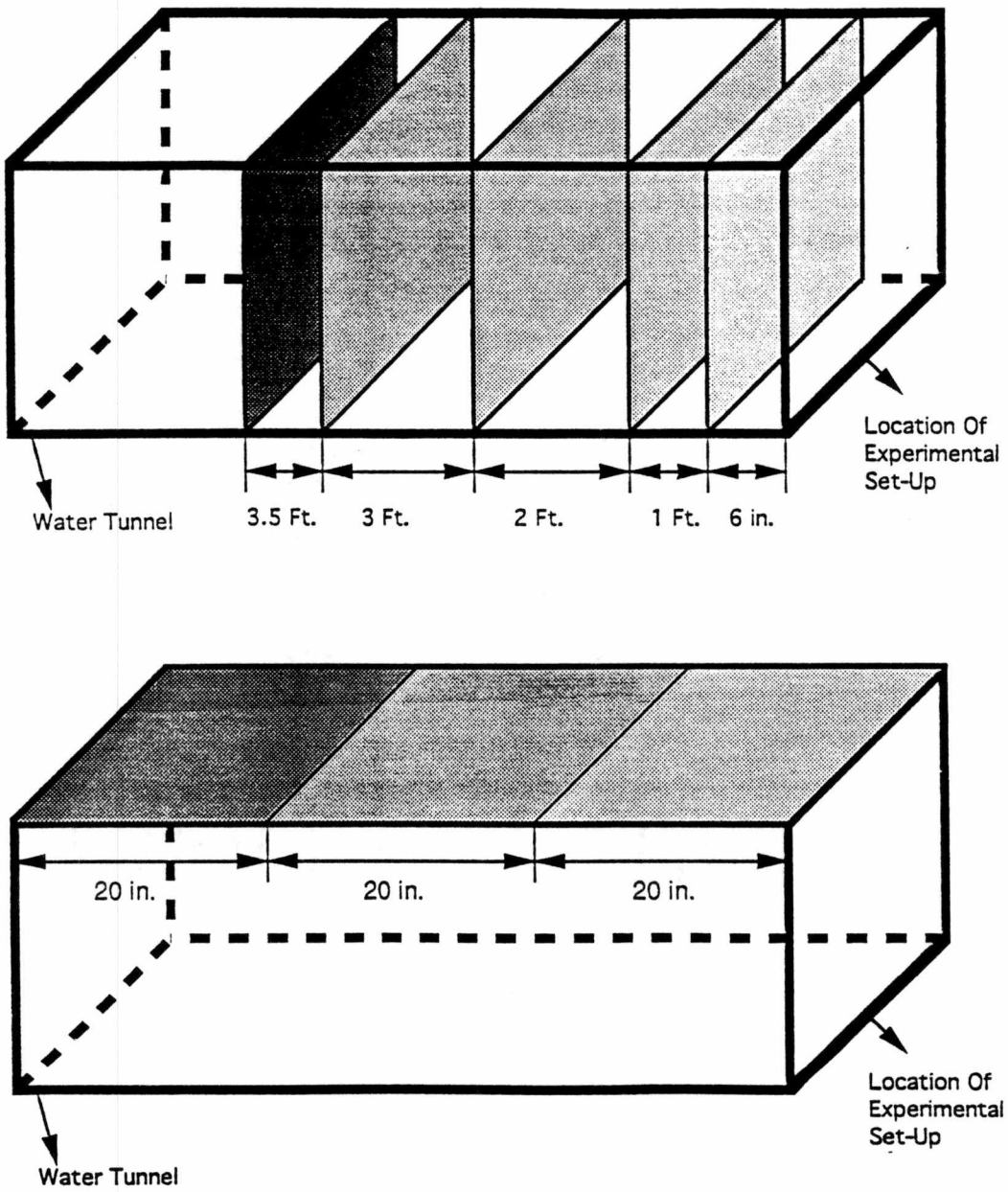

Fig. 27. Location at which qualitative data is recorded.

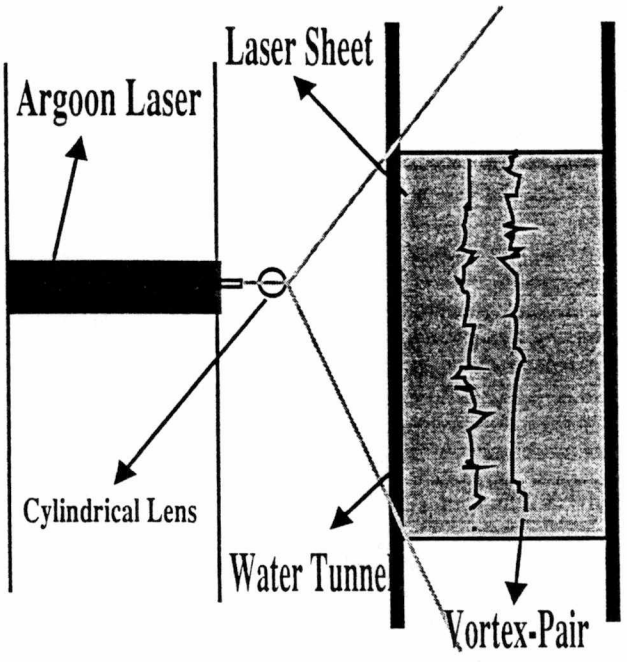

a) Top view.

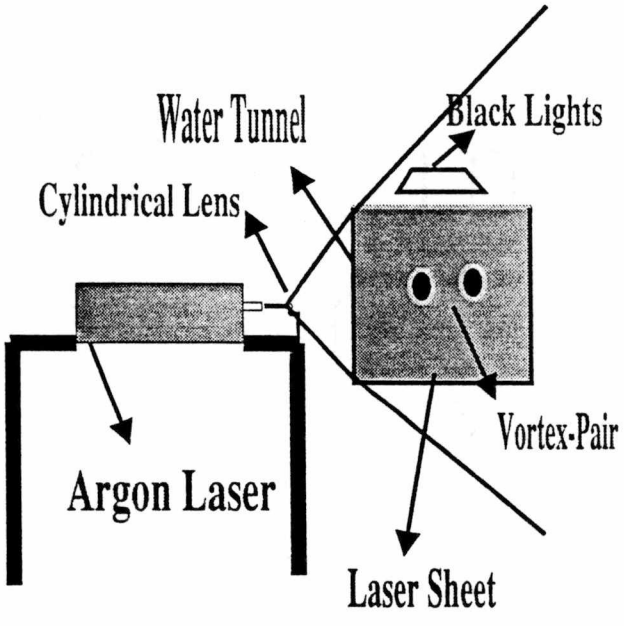

b) Side view.

Fig. 28. Laser sheet configuration. The laser highlights the counter rotating vortex pair.

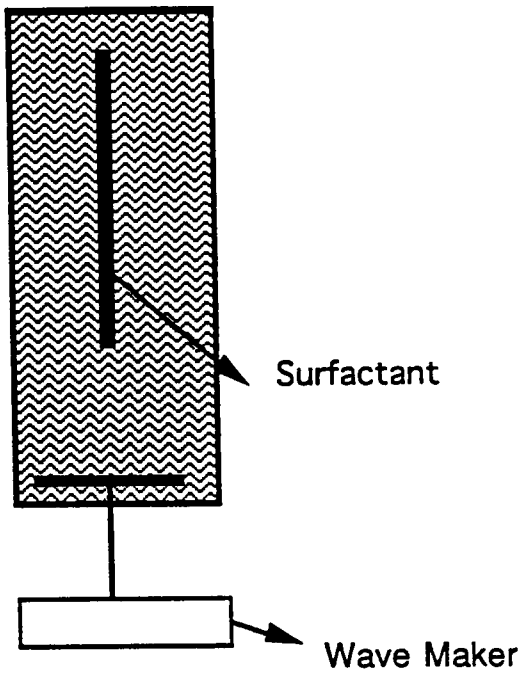

Liquid	Surface Tension (N/m)
- Ammonia	2.13
- Ethanol	2.28
- Gasoline	2.16
- Kerosine	2.8
- Glycerin	6.33
- SAE 30 Oil	3.5
- Water	7.28
- Seawater	7.28

Fig. 29. Surface tension effects. Preliminary settings.

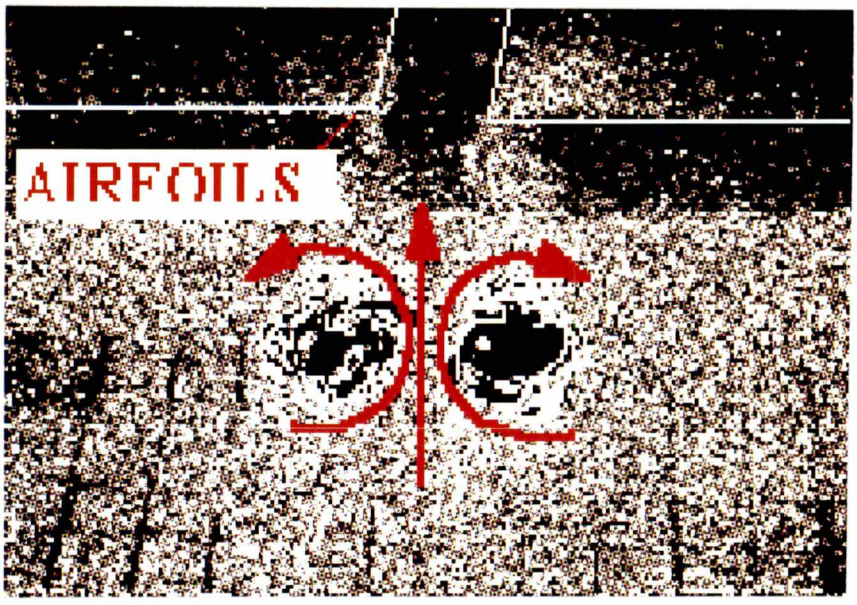

a) 6 in.



b) 3.0 ft.

Fig. 30. Evolution and development of vortex pair. (Do/bo=1.72, αo=10, V=5 in./s.).



c) 3.5 ft.

Fig. 30. (continued).

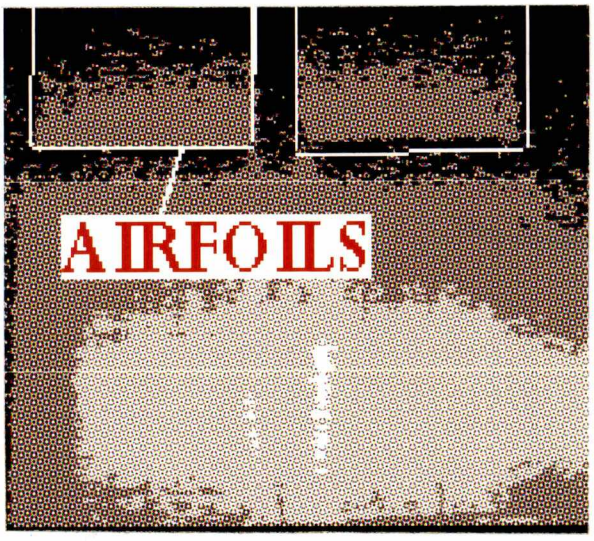

a) First section. No disturbances.

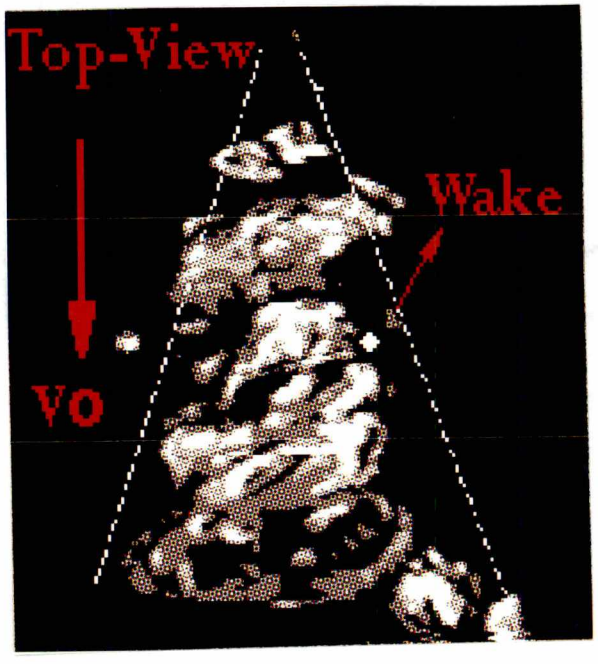

b) Second section. Vortices arrive to free surface.

Fig. 31. Development of surface signature. (Do/bo=1.72, αo=10, V=5 in./s.).

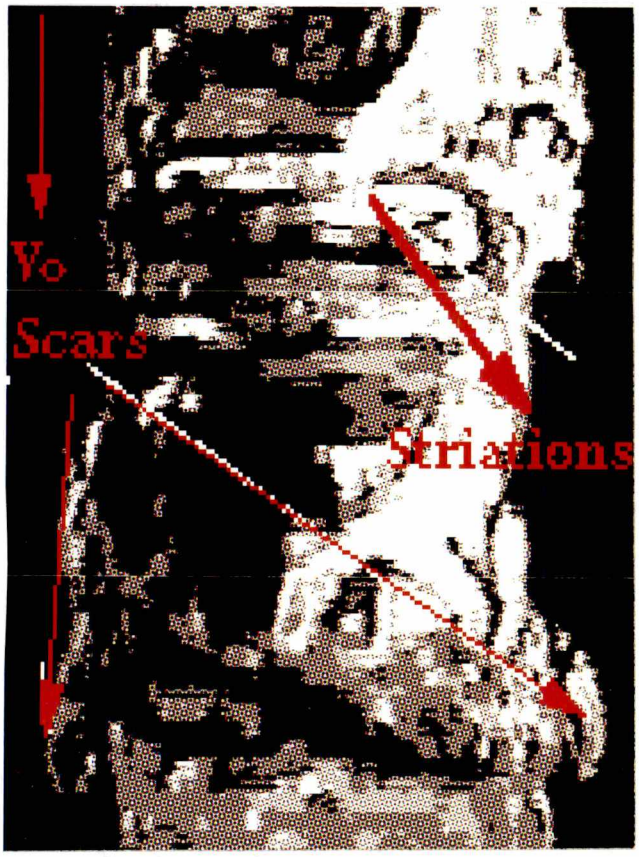

a) Completely developed surface vortex interaction.

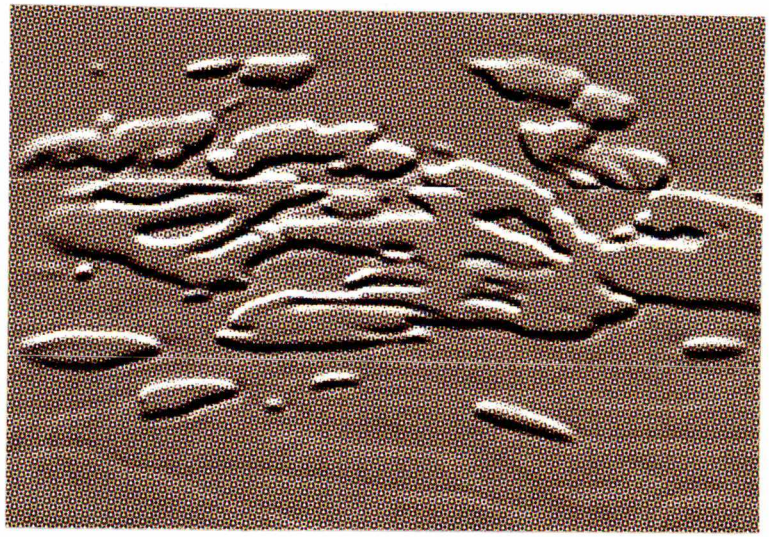

b) Initial 3-D disturbances.

Fig. 32. 3-D surface signature. (Do/bo=1.72, αo=10, V=5 in./s.).

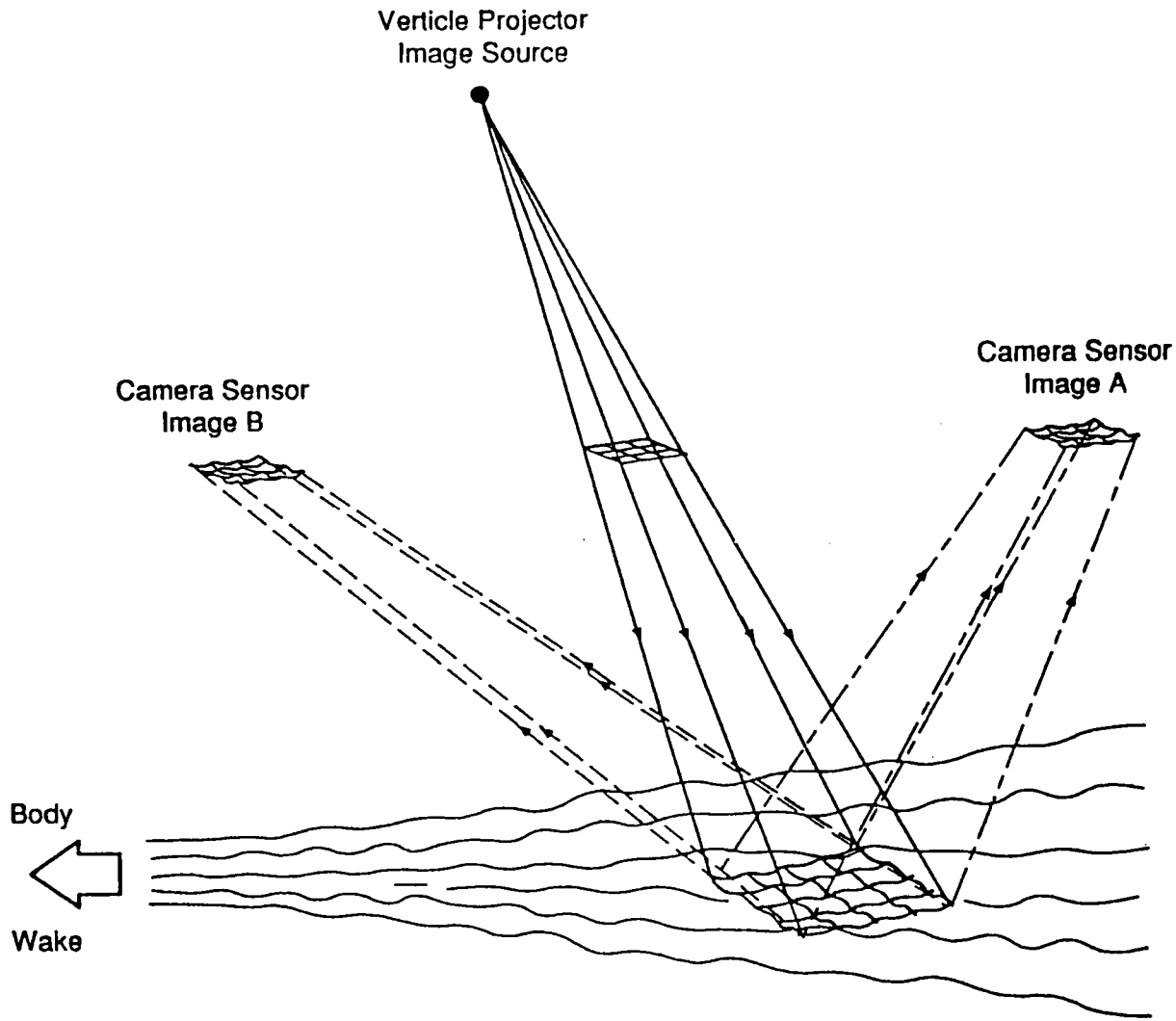

Fig. 33. Schematic, Optical Topographic Mapping.

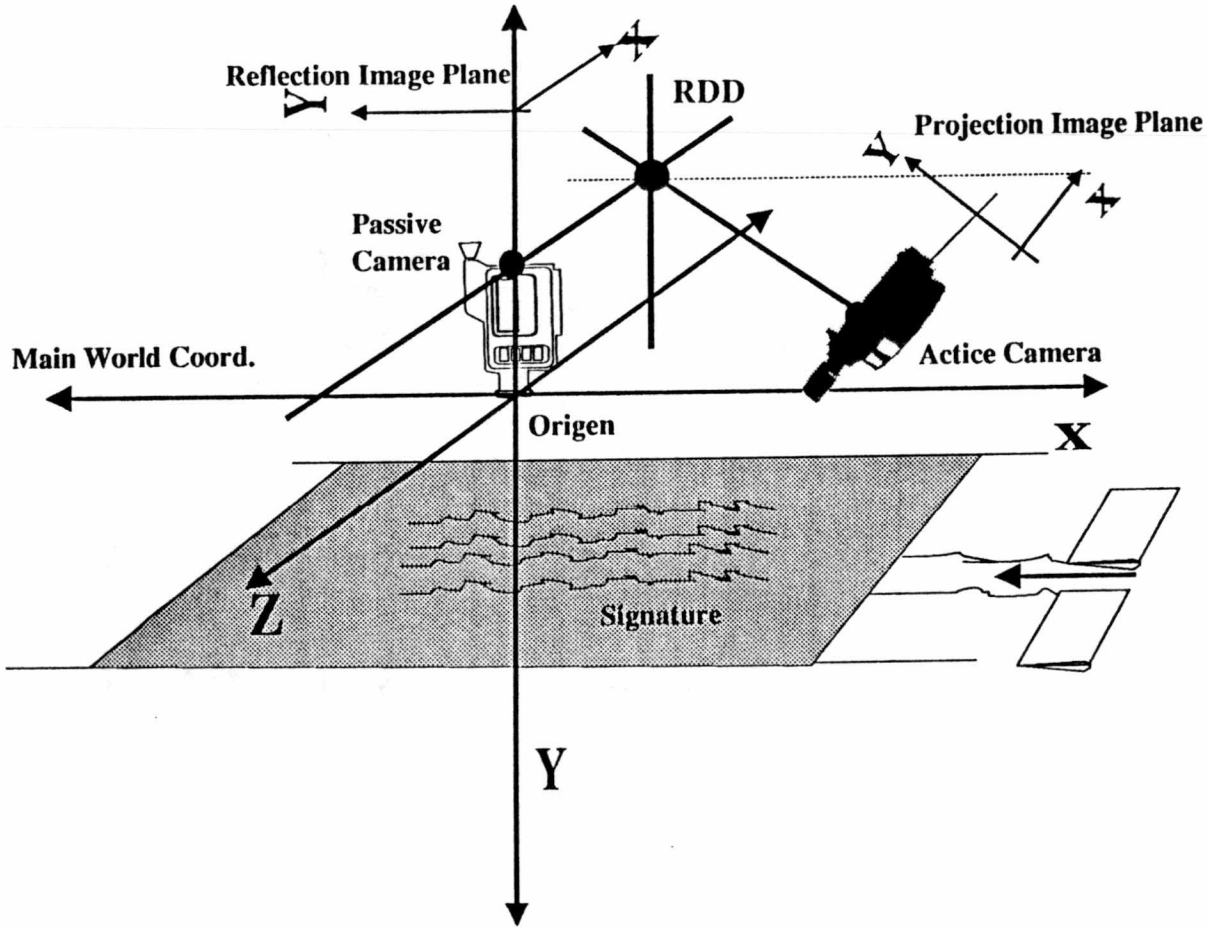

Fig. 34. Experimental, Optical Topographic Mapping.

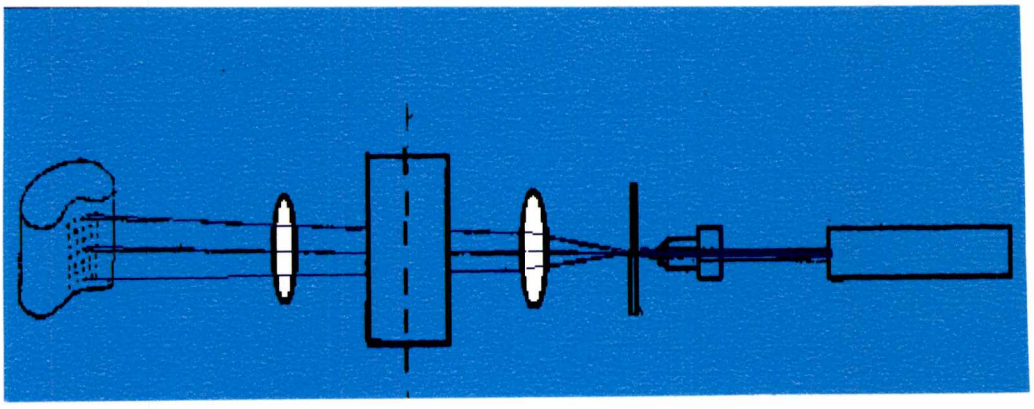

Fig. 35. Active camera. Projects a Laser beam array.
Source: Taboada J., Altschuler B. R., United States Patent files, Patent # 4,523,809, June 18, 1985.

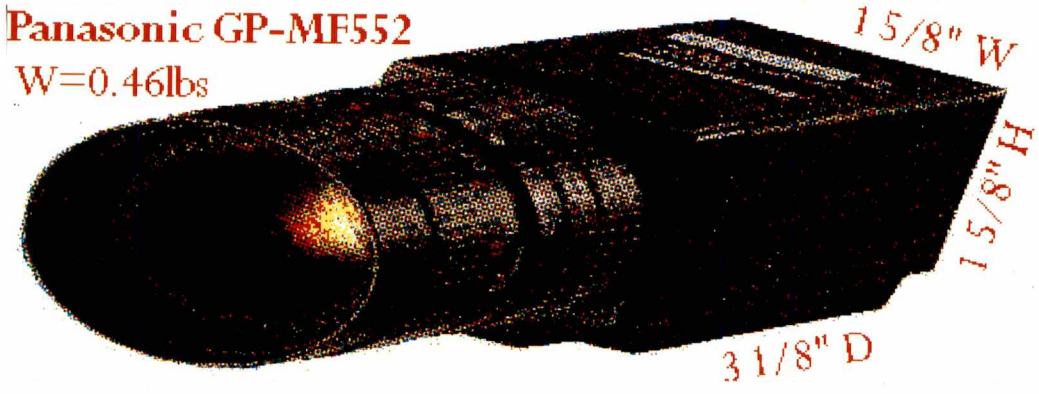

Fig. 36. Passive Camera. CCD camera. Captures the reflection.

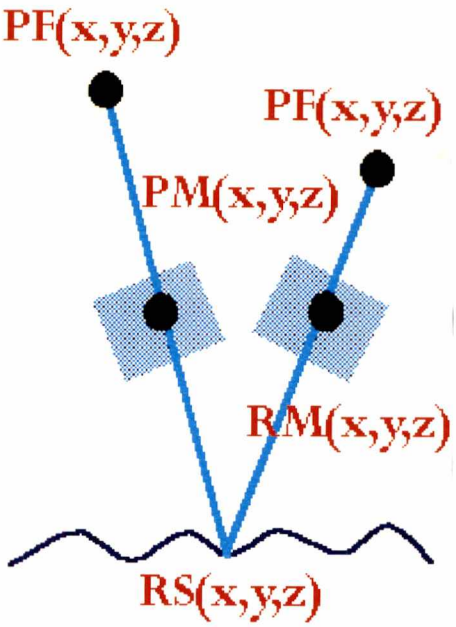

Fig. 37. Mathematical Coordinates, Optical Topographic Mapping. Single Ray.

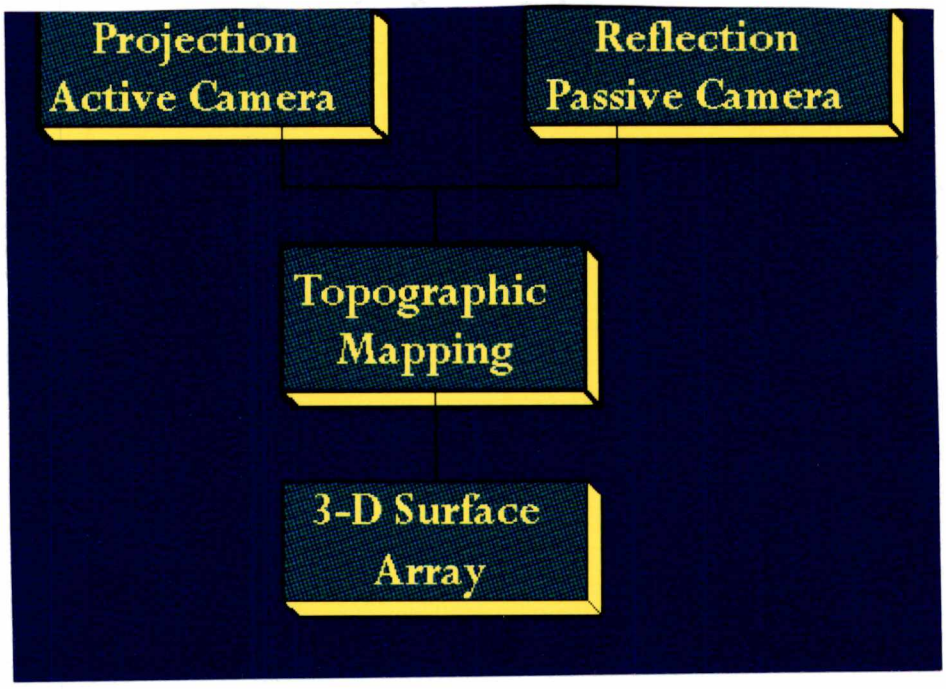

Fig. 38. Basic reconstruction algorithm.

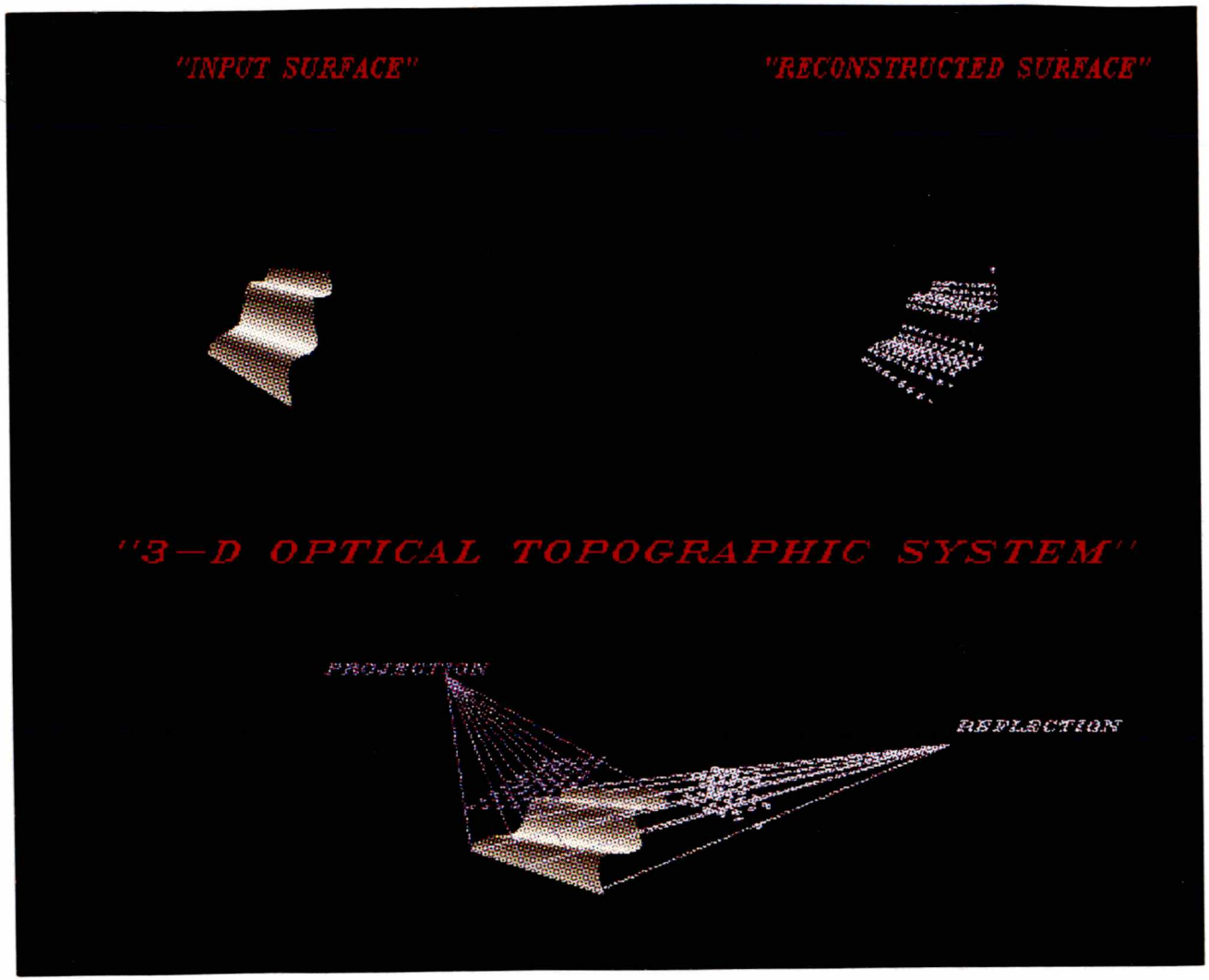

Fig. 39. Simulation, "3DOTS", Three Dimensional Optical Topographic System.

2. LIST OF TABLES

Table I. Vortex Rotation. Experimental model.

WING SECTION	ANGLE OF ATTACK	ROTATION
Right	+	c.w.
Right	-	c.c.w.
Left	+	c.c.w.
Left	-	c.w.

Table II. Simulation parameters.

Workable Parameters Simulation

Do= Distance From Surface. Vt= Velocity Of Tunnel

bo= Initial Vortex Separation A.A.= Angle Of Attack

Input Parameters:

Chord : [in] 5

Span: [in] 6

Do	bo	Vt	A.A.	Lift Coefi-cient	Circula-tion Initial	Circula-tion	Induced Vortex Velocity	Time Reach Surface	Distance Horizon-tal	Froude Number
[in]	[in]	[in]/s	Deg.	[ ]	in**2/s	in**2/s	[in]/[s]	[s]	[in]	[ ]
0.5	0.5	5	14	1.42	17.75	7.46	3.02	0.17	0.83	0.25
0.75	0.5	5	14	1.42	17.75	7.46	3.02	0.25	1.24	0.25
1	0.5	5	14	1.42	17.75	7.46	3.02	0.33	1.65	0.25
1.5	0.5	5	14	1.42	17.75	7.46	3.02	0.50	2.48	0.25
2.5	0.5	5	14	1.42	17.75	7.46	3.02	0.83	4.14	0.25
3.5	0.5	5	14	1.42	17.75	7.46	3.02	1.16	5.79	0.25
0.5	0.7	5	14	1.42	17.75	7.46	2.16	0.23	1.16	0.15
0.75	0.7	5	14	1.42	17.75	7.46	2.16	0.35	1.74	0.15
1	0.7	5	14	1.42	17.75	7.46	2.16	0.46	2.32	0.15
1.5	0.7	5	14	1.42	17.75	7.46	2.16	0.70	3.48	0.15
2.5	0.7	5	14	1.42	17.75	7.46	2.16	1.16	5.79	0.15
3.5	0.7	5	14	1.42	17.75	7.46	2.16	1.62	8.11	0.15

Table III. Sample of testing parameters employed during the experiments.

αo		Do		bo	Vo
Degrees		in.		in.	in./s
Left	Right	Left	Right		
10	10	3. 13/16	3. 13/16	1. 3/8	2.4
10	10	3. 13/16	3. 13/16	1. 3/8	5.4
10	10	3. 13/16	3. 13/16	2 3/8	2.4
10	10	3. 13/16	3. 13/16	2 3/8	5.4
10	10	3. 9/16	3. 9/16	2 3/8	5.5
10	10	3. 9/16	3. 9/16	1 3/8	2.4
10	10	2.	2.	1 1/8	2.4
10	10	2.	2.	2 3/8	5.4
10	10	2.	2.	2 3/8	5.4
10	10	3.	3.	1 3/4	3.5

VITA

Alfredo Gabrie was born in Honduras, Central America on December 17, 1969. He attended elementary schools in Honduras and graduated from a Jesuit High School in December 1986. The following January he started an Intensive English Program in Colorado State University. He received a Bachelor of Science in Mechanical Engineering from Tennessee Technological University in May 1992.